Regular Simplex Hierarchical Gravity Part III: Hierarchical Renormalization and the 600-cell as a Separation Device

Ryuhei Sato[1,*]

[1] *Independent Researcher, Tokyo, Japan*

(Dated: June 9, 2026)

Parts I and II established the static geometry and the dynamics of Regular Simplex Hierarchical Gravity (RSHG): from Axiom Zero and the ineliminable tetrahedral packing deficit $\delta = 2\pi - 5\arccos(1/3) \approx 7.36^\circ$ (Niven's theorem), the 600-cell arises as the unique four-dimensional closure, and its projection onto the three-dimensional brane yields gravity ($\Omega_{\text{local}} \approx 100$, reproducing G to 1.1%) together with the Light-Speed Resource Allocation Principle $c^2 = v^2 + \tau^2$. Part III develops the thermodynamics of this structure. We assign the 600-cell a second role, as a separation device that, at every hierarchy boundary, partitions the incoming frustration into three mutually exclusive channels—structural stress (rigidity transmitted upward), computational entropy (heat dissipated downward, the arrow of time), and unresolved four-dimensional residue (a dark-matter candidate)—under the conservation of frustration $\Phi_{\text{in}} = \Phi_A + \Phi_B + \Phi_C$. We then establish the central identity of the paper: time-averaging the vibrating force chains over a time scale τ is equivalent to spatial coarse-graining over a length $c\tau$, which is exactly a renormalization operation, so that the observation time scale itself selects the observed hierarchy. Iterating this renormalization across six hierarchies—each a jamming transition forced by the capacity limit of frustration, with a scale ratio of 10^6 and a per-step rigidity transmission $\varepsilon_n \approx 10^{-19.2}$—produces a cumulative suppression $\varepsilon_{\text{total}} \approx 10^{-115.2}$ that approaches the 122-order cosmological-constant discrepancy as an arithmetic consequence, while $\phi \approx 0.62$, $\Omega_{\text{local}} \approx 100$, and $\delta \approx 7.36^\circ$ remain invariant at every scale. Finally, we analyze the dynamic stability of that operating point, where gravity (structural stress) and Pauli repulsion (computational entropy) balance just inside the packing limit: the universe never reaches ϕ_c, and the residual structural vacancy $\phi_c - \phi \approx 0.02$ simultaneously averts asymptotic freezing, sustains the renormalization dynamics, and serves as the leak path through which force reaches three dimensions. A system poised at this boundary between structural stress and computational entropy offers a physical perspective on the boundary conditions that may sustain complex systems such as life. We state explicitly which quantities are fixed with zero free parameters and which—notably the first-principles value of ε_n—remain open.

I. INTRODUCTION

A. Connection to Parts I and II

In Part I, Axiom Zero was formulated as the unification of quantum entanglement and the Pauli exclusion principle as two faces of the same mathematical fact. The impossibility of filling three-dimensional space with regular tetrahedra was established as an algebraic necessity through Niven's theorem [1], and the deficit angle $\delta = 2\pi - 5\arccos(1/3)$ was shown to be an ineliminable topological residue with transcendental properties. The escape route into four dimensions through this topological residue is the 600-cell, whose projection into three dimensions manifests as force chains—the observed forces. The effective vertex count $\Omega_{\text{local}} = 100.000069$ was derived with zero free parameters, achieving a 1.1% agreement with the observed gravitational constant G.

In Part II, dynamics were derived from this static geometric structure. The speed of light was reformulated as the bandwidth upper limit of the computational network, and the Light-Speed Resource Allocation Principle (LRAP) $c^2 = v^2 + \tau^2$ was established as the orthogonal allocation between spatial propagation v and internal state maintenance τ. Mass was reinterpreted as projection caustics, force as the spatial gradient of the frustration potential, and singularities as dimensional arrest. In the final section, the necessity of hierarchical phase transitions was anticipated through the monotonic accumulation of the non-zero topological conserved quantity, as guaranteed by the Gauss–Bonnet theorem, when the effective packing fraction ϕ approaches the jamming criticality $\phi_c \approx 0.64$.

Part III develops this anticipated hierarchical phase transition through informational thermodynamics. The central question is: why does a consistent geometric rule persist across hierarchies, even though discontinuous phase transitions occur at every hierarchy boundary?

B. Central Question: The Coexistence of Discontinuity and Consistency

Hierarchical structure is observed at every scale in physics. The transition from quarks to protons, from atoms to molecules, from cells to tissues, from rock to crustal blocks, from planets to planetary systems, from

* ryuhei19691001@gmail.com

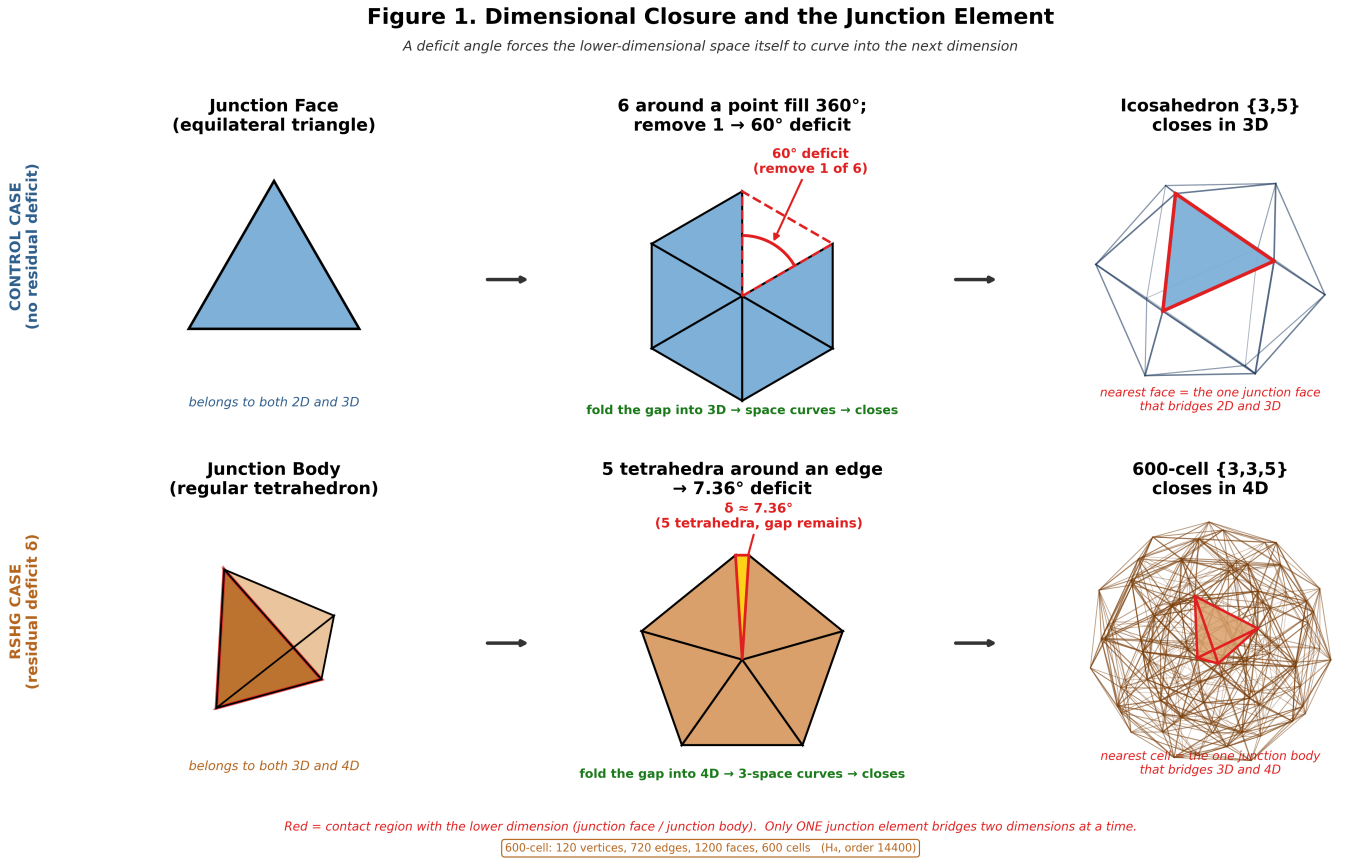

FIG. 1. **Dimensional Closure and the Junction Element.** A deficit angle forces the lower-dimensional space itself to curve into the next dimension. In the control case (top) six equilateral triangles fill 360° around a point; removing one leaves a 60° deficit that closes with zero residue into the icosahedron $\{3, 5\}$ in 3D. In the RSHG case (bottom) five regular tetrahedra around an edge leave the irreducible deficit $\delta \approx 7.36°$ (Niven's theorem), which closes only in 4D, as the 600-cell $\{3, 3, 5\}$; red marks the single junction element that bridges the two dimensions. *Note on causality:* the panels are arranged bottom-up—"a 3D gap appears, so space curves into 4D"—purely as an aid to intuition. In RSHG the true order is top-down: the four-dimensional symmetry of the 600-cell is the stable, primary structure, and the 3D deficit is merely what a three-dimensional observer registers once that structure is projected and packed. Figure 1 therefore illustrates the order of understanding—the geometric premise of what follows—not the order of being.

galaxies to galaxy clusters—at each of these boundaries, the degrees of freedom of the lower hierarchy are reorganized into the effective degrees of freedom of the upper hierarchy. According to the general theory of jamming transitions [2, 3], this reorganization is fundamentally a discontinuous phase transition.

However, a consistent rule persists across these hierarchies. At each hierarchy, the effective packing fraction $\phi \approx 0.62$ is universally observed, the local structure with effective vertex count $\Omega_{\text{local}} \approx 100$ is reproduced, and the topological residue $\delta \approx 7.36°$ is preserved across all hierarchies.

This fact admits two interpretations. The first interpretation attributes the consistency to coincidence: each hierarchy independently arrives at similar geometric conditions. This is an uneconomical explanation relying on chance. The second interpretation posits a single geometric mechanism operating across hierarchies, of which the discontinuous phase transitions at each boundary are only local manifestations. This paper adopts the second interpretation and formulates the mechanism as coarse-graining through time-averaging.

C. Central Claim: The Identity of Time-Averaging and Renormalization

The central claim of this paper is expressed as the following identity. Time-averaging, coarse-graining, renormalization, and scaling law—these four operations are different aspects of the same physical process. Specifically, time-averaging the configurations of vibrating force chains at the lower hierarchy over a time scale τ is equivalent to coarse-graining spatially over a length scale $c\tau$. This operation functions as a renormalization operation, and as a result, the consistent rule across hierarchies is observed as a scaling law.

This identity is a natural consequence of the Light-

Speed Resource Allocation Principle established in Part II. The LRAP describes the bandwidth allocation between two computational tasks; this paper shows that its integration along the time direction generates hierarchical structure.

D. The Two Functions of the 600-cell

Throughout Parts I and II, the 600-cell functioned as a transducer translating four-dimensional geometric tension into three-dimensional forces. In this paper, we introduce a second function in addition to this transducing function: the function as a separation device that, at each hierarchy boundary, separates the input total frustration into structural stress (transmitted as rigidity to the upper hierarchy) and computational entropy (dissipated as heat to the lower hierarchy).

This separation function is a refinement, in the context of hierarchical renormalization, of the bifurcation of the topological residue anticipated in Section IV.A of Part I. The physical units of separation are based on the geometric role division of the four attributes (vertices, edges, faces, bodies), with the body (three-dimensional cell) functioning as the unit of rigidity.

E. Observation Time Scale and the Observed Hierarchy

A natural consequence derived from the framework of this paper is the structure in which the observation time scale determines the observed hierarchy. In a system observed with observation time τ_{obs}, the reconfigurations of force chains proceeding at time scales faster than τ_{obs} are averaged out and become invisible. Conversely, structural changes slower than τ_{obs} appear as a static background. Therefore, depending on the observation time scale, the structure of the corresponding hierarchy emerges as the object of observation.

This consequence provides a methodological guideline in cosmological observation. The composition of the universe (the ratio of dark matter, visible matter, and dark energy) is the structure at the largest hierarchy, and is therefore understood as a quantity determined at the longest observation time scale (the time scale of the age of the universe).

F. Current Status and Limitations of Zero-Parameter Derivation

This paper theoretically presents the structure of hierarchical renormalization and shows that renormalization across six hierarchies is consistent with the observed cosmological constant problem (a discrepancy of 122 orders of magnitude). The existence of the suppression ratio $\varepsilon_n \approx 10^{-19.2}$ per hierarchy and the structure by which it accumulates across six hierarchies are naturally derived from the framework of this paper.

However, a first-principles derivation of the specific numerical value of ε_n has not been completed within the scope of this paper. At present, this value is characterized by an inverse calculation from observed values and consistency with the empirical critical exponents of jamming physics. A complete first-principles derivation remains as a subject for future research. This paper explicitly records this incompleteness and presents it with intellectual honesty.

G. Structure of This Paper

In Section II, the geometric attributes of the 600-cell (vertices, edges, faces, bodies) are completed, and the two functions of transducer and separation device are introduced. The geometry of boundary surfaces and hierarchical coupling is positioned as the origin of the strength differences of forces across hierarchies.

In Section III, the dynamic picture of vibrating force chains is presented. The vibration as the physical implementation of the NP-hard reconfiguration problem and the operation of the separation device through its time-averaging are described.

In Section IV, the central claim of this paper—the identity of time-averaging and renormalization—is established. The correspondence between observation time scale and the observed hierarchy is formulated.

In Section V, the structure of six-hierarchy renormalization is presented. The ratio of rigidity transmission and heat dissipation at each hierarchy, the accumulation across six hierarchies, and the approach to the cosmological constant problem are discussed. The current status and limitations of first-principles derivation are explicitly stated.

In Section VI, the scope of applications suggested by the framework of this paper is presented as a broad overview across scales, from quantum to galactic.

In Section VII, the stability of the operating point $\phi \approx 0.62$ is discussed. The balance between gravity and Pauli repulsion, the boundary definition of life, and the prediction of rigidity inhomogeneity at the uppermost hierarchy are developed.

In Section VIII, the integration of the entire trilogy and the scope of future research are presented.

II. COMPLETION OF THE GEOMETRIC ATTRIBUTES OF THE 600-CELL AND ITS TWO FUNCTIONS

A. The Three Attributes in Part II and Their Role Division

In Section V.A of Part II, when the regular tetrahedron was adopted as the fundamental unit of three-

dimensional space, the following role division was established for its geometric dimensional elements. Vertices (zero-dimensional) function as the positions of computational nodes, edges (one-dimensional) function as the propagation of quantum phases and vibrational modes, and faces (two-dimensional) function as the interfaces of frustration propagation. Force was defined as the spatial gradient of frustration propagating in the normal direction of faces.

This framework of three attributes was necessary and sufficient for the theoretical development of Parts I and II. The derivation of the gravitational constant, the establishment of the Light-Speed Resource Allocation Principle, and the reinterpretation of singularities as dimensional arrest—all were completed within the role division of vertices, edges, and faces.

However, in discussing hierarchical renormalization, this framework is insufficient. To distinguish between the transmission of rigidity and the dissipation of heat at hierarchy boundaries, it is necessary to introduce the role of the body (three-dimensional cell) as a fourth attribute in earnest.

B. The Body as the Fourth Attribute

The body (three-dimensional cell) is positioned in this paper as the unit of rigidity. It is also the container of the topological residue δ.

In Section V.A of Part II, the three-dimensional content of the regular tetrahedron was already mentioned as "the container of the topological residue δ." This paper develops this further and shows that the body functions as the unit of rigidity transmission at hierarchy boundaries.

The role division of the four attributes is summarized in Table I.

Through this completion of the four attributes, this paper inherits the theoretical foundations of Parts I and II while acquiring the complete geometric vocabulary necessary to describe hierarchical renormalization.

C. Topological Boundary Surfaces and the Leak Path of Force

As a direct consequence of introducing the concept of the body, a distinction emerges as to whether the unit structure of each hierarchy is closed or not.

A completely closed body retains the topological residue δ entirely within its interior. Since no boundary surface exists, the internal frustration does not leak to the outside. A unit structure in this state is determined as an "object" independent of the three-dimensional observer, and is mechanically static with respect to the exterior. In contrast, a body with a boundary surface leaks the internal frustration to the outside through that boundary surface. The boundary surface functions as a leak path of force. That is, in a unit structure with incomplete packing and a remaining geometric gap (boundary surface), the topological residue accumulated in the interior manifests as a "force (physical interaction)" into three-dimensional space through this gap. The observed forces—the strong force, electromagnetic force, gravity, and others—are all manifestations of this "leakage" at different scales.

Here we must recall the conservation of the topological residue guaranteed by the Gauss–Bonnet theorem. In Section IV.A of Part I, it was shown that the total topological residue δ is fixed as a conserved quantity on a closed manifold. Therefore, the complete closure of a unit structure does not mean that the internal δ is locally eliminated. δ is merely locally confined, and its leakage to the outside is blocked.

From this perspective, the completion of packing is formulated as follows. The completion of packing is the elimination of the topological boundary surface, which appears to a three-dimensional observer as the determination as an object, and in relation to the four-dimensional structure as the disconnection from four dimensions. Both are two aspects of the same operation.

D. The Hierarchical Decrease in Closure Cost

At each hierarchy, the operation of closing the boundary surface of a unit structure involves a geometric cost. This cost is quantified as the structural tension required to locally confine the internal topological residue δ.

As an important property, the closure cost decreases as the hierarchy ascends. The unit structures of lower hierarchies (such as protons) require large costs for boundary closure, which manifests as the strength of the strong force. The unit structures of upper hierarchies (such as galactic halos) have small closure costs, which manifests as the weakness of gravity. The structure in which the closure cost decreases by a ratio of $\varepsilon_n \approx 10^{-19.2}$ as the hierarchy ascends is the geometric origin of the strength difference between the strong force and gravity observed in Part I (a gap of 10^{39} orders of magnitude).

The progression of closure has the effect of reducing the frustration-processing cost of the entire universe. When a boundary surface closes, the necessity of continuously suppressing the internal δ from the outside disappears. This saving appears as a local dissipation of computational entropy generated at each hierarchy. The difference between the closure cost and the amount of saving determines the net thermodynamic balance at that hierarchy.

E. The Two Functions of the 600-cell

Based on the discussion thus far, the function of the 600-cell in this paper is formulated in two stages.

Attribute	Dimension	Role
Vertex	0	Position of computational node; mass
Edge	1	Quantum phase propagation; vibrational mode
Face	2	Interface of frustration propagation; hinge of force
Body	3	Unit of rigidity; container of topological residue δ

TABLE I. The role division of the four attributes of the 600-cell.

a. First Function: The Transducer. As established throughout Parts I and II, the 600-cell functions as a transducer that translates four-dimensional geometric tension into three-dimensional forces (force chains). This function is described as the process by which structural stress is generated through the projection into three dimensions from the cooperative arrangement of 600 regular tetrahedra in four-dimensional space. The derivation of the gravitational constant G in Part I is the quantitative consequence of this transducing function.

b. Second Function: The Separation Device. As a function newly introduced in this paper, the 600-cell functions as a separation device that, at each hierarchy boundary, separates the input total frustration into structural stress (the component transmitted to the upper hierarchy as rigidity) and computational entropy (the component dissipated to the lower hierarchy as heat). The input and output of the separation device are formulated as follows: the input is the unprocessed frustration arriving from the lower hierarchy (the accumulation of topological residue δ); Output 1 (structural stress) is the rigidity transmitted to the upper hierarchy through the closure of boundary surfaces; and Output 2 (computational entropy) is the computational heat dissipated in the closure process.

This separation function is a refinement, in the context of hierarchical renormalization, of the bifurcation of the topological residue anticipated in Section IV.A of Part I. Both functions (transducing and separation) are derived from the same geometric structure of the 600-cell, and the two functions are understood as different aspects of the same mathematical fact.

F. Exact Geometric Invariants Hidden in the Projection of the 600-cell

As the mathematical foundation supporting the two functions of the 600-cell, we present exact geometric invariants hidden in the process of its projection into three dimensions. These invariants emerge as algebraic consequences of the H_4 symmetry (order 14,400) and are all expressed as exact rational numbers or as algebraic integers containing the golden ratio $\phi = (1+\sqrt{5})/2$.

a. Higher Moments of Edge Projection Probability. Through direct algebraic computation based on the H_4 symmetry of the 600-cell, the invariants $\langle \sin^2\theta_e \rangle = 3/4$ and $\langle \cos^2\theta_e \rangle = 1/4$ for the projection of the 720 edges are established. This paper extends this to higher moments.

$$\langle \cos^2\theta_e \rangle = \frac{1}{4}, \quad \langle \cos^4\theta_e \rangle = \frac{1}{8}, \quad \langle \cos^{10}\theta_e \rangle = \frac{21}{512} \tag{1}$$

All of these values are rigorously derived from the combinatorial structure of the five orbits (180 edges, 144 edges, 240 edges, 144 edges, 12 edges) into which the edges are classified by the H_4 symmetry. All values are exact rational numbers, and terms containing $\sqrt{5}$ vanish through symmetric cancellation.

As a particularly important consequence, the expected value of the squared projection preservation rate of edges is computed as follows.

$$\langle \sin^4\theta_e \rangle = 1 - 2\langle \cos^2\theta_e \rangle + \langle \cos^4\theta_e \rangle = 1 - \frac{1}{2} + \frac{1}{8} = \frac{5}{8} \tag{2}$$

This value $5/8 = 0.625$ lies in the immediate vicinity of the operating point $\phi \approx 0.62$ observed in jamming physics. The fact that the value 5/8 emerges directly as an exact rational number from the geometry of the 600-cell is one piece of strong evidence suggesting the geometric origin of the operating point in this paper. However, asserting $5/8 = \phi_c$ is impossible at the present time, and its identification requires future theoretical refinement. This point will be discussed again in Section VII.[17]

b. A New Invariant: Face Projection Probability. While in earlier parts of this work only invariants related to edge projection were discussed, this paper newly establishes invariants related to face projection. For the 1,200 faces (all equilateral triangles) of the 600-cell, we consider the squared area-preservation rate $\sin^2\theta_{\text{face}}$ of each face when projected into three-dimensional space. Here, $\sin^2\theta_{\text{face}}$ is defined as the square of the ratio of the area of the three-dimensional projected image to the area of the face in four dimensions.

Through direct computation, the 1,200 faces are classified into six orbits, and the values of $\sin^2\theta_{\text{face}}$ in each orbit are exactly determined. The average of these values is calculated as follows.

$$\langle \sin^2\theta_{\text{face}} \rangle = \frac{1}{2} \tag{3}$$

The exactness of this value is confirmed in two ways. First, through the combinatorial computation of the six orbits based on H_4 symmetry, it is confirmed that terms containing $\sqrt{5}$ completely cancel out.[18] Second, it is independently derived as $\binom{3}{2}/\binom{4}{2} = 3/6 = 1/2$ from the general theorem on the expected value of the squared

area of a two-dimensional figure projected from four-dimensional space onto a three-dimensional subspace (a special case of the Furstenberg–Tzkoni integral-geometry formula [9]).

$\langle \sin^2 \theta_{\text{face}} \rangle = 1/2$ is an exact geometric invariant for faces, on par with $\langle \sin^2 \theta_e \rangle = 3/4$ for edges. This is a result newly established in this paper, and it provides the foundation for faces to function as the geometric units of rigidity transmission in the separation device.

c. Structural Correlation between Edges and Faces. Edges and faces are not independent geometric elements; each edge has five faces sharing it (a geometric consequence of the uniform cluster coefficient 5/11 of the 600-cell). Therefore, a structural correlation exists between the projection of edges and the projection of faces. Denoting the average projection-preservation rate of the five faces adjacent to each edge as $\langle \sin^2 \theta_f \rangle_{\text{adjacent}}$, the following proportional relation holds between this and the projection-preservation rate of the edge itself, $\sin^2 \theta_e$.

$$\langle \sin^2 \theta_f \rangle_{\text{adjacent}} = \frac{2}{3} \sin^2 \theta_e \tag{4}$$

This proportional relation reflects an essential symmetry in the geometric connection between edges and faces. The proportionality coefficient 2/3 is derived from the dimensional constraints in the projection of edges (one-dimensional) and faces (two-dimensional).

Using this proportional relation, the expected value of the product of the preservation rates of edges and faces is exactly computed as follows.

$$\left\langle \sin^2 \theta_e \cdot \langle \sin^2 \theta_f \rangle_{\text{adjacent}} \right\rangle = \frac{2}{3} \langle \sin^4 \theta_e \rangle = \frac{2}{3} \cdot \frac{5}{8} = \frac{5}{12} \tag{5}$$

This value 5/12 is greater than the product $\langle \sin^2 \theta_e \rangle \cdot \langle \sin^2 \theta_f \rangle = (3/4)(1/2) = 3/8$, which would hold under the assumption of independence between edges and faces. The difference between the two manifests as a positive covariance.

$$\text{Cov}\big(\sin^2 \theta_e,\ \langle \sin^2 \theta_f \rangle_{\text{adjacent}}\big) = \frac{5}{12} - \frac{3}{8} = \frac{1}{24} \tag{6}$$

The covariance 1/24 is also an exact rational number, serving as a quantitative indicator that edges and faces exhibit geometrically coordinated preservation patterns.

d. Volume Ratio as a Snapshot. To observe the operation of the separation device in units of bodies (three-dimensional cells), we consider the ratio of the 3-volume V_{4D} of each regular tetrahedron in four-dimensional space to the 3-volume V_{3D} of its three-dimensional projected image with respect to a specific projection direction. For the 600 regular tetrahedra of the 600-cell, the average of $(V_{3D}/V_{4D})^2$ is computed as follows.

$$\left\langle \left(\frac{V_{3D}}{V_{4D}} \right)^2 \right\rangle = \frac{1}{4} \tag{7}$$

This value coincides with $\langle \cos^2 \theta_e \rangle = 1/4$ for edges. This is not a coincidence but a consequence of general statistical properties of projection under H_4 symmetry.

However, an important caveat must be noted regarding the volume ratio. The distribution of the volume ratio is discretely classified depending on the projection direction (the 600 regular tetrahedra are classified into 8 orbits), but this classification itself depends on the projection direction. When the projection direction changes, which regular tetrahedron belongs to which orbit changes. In contrast, the statistical structure of the orbits (the number of orbits, the distribution of the number of regular tetrahedra in each orbit, the average values) does not depend on the projection direction. Therefore, in this paper, the volume ratio is positioned as a snapshot at a single computational step. The essential operation of the separation device lies not in this instantaneous volume ratio but in the process of time-averaging and coarse-graining introduced in Section IV.

G. Summary of This Section

In this section, the completion of the four attributes—achieved by adding the body (three-dimensional cell) to the three attributes (vertices, edges, faces) established in Parts I and II—was accomplished. The body functions as the unit of rigidity and the container of the topological residue δ, and the closure of its boundary surface was formulated as the completion of packing.

The 600-cell has two functions. In addition to the function as a transducer (Parts I and II), this paper introduced the function as a separation device. The separation device, at each hierarchy boundary, separates the input total frustration into structural stress and computational entropy.

As the mathematical foundation supporting these functions, multiple exact geometric invariants derived from H_4 symmetry were presented. $\langle \sin^2 \theta_{\text{face}} \rangle = 1/2$ is an invariant newly established in this paper, and $\langle \sin^4 \theta_e \rangle = 5/8$ is positioned as a candidate for the geometric origin of the operating point $\phi \approx 0.62$. The proportional relation 2/3 between edges and faces and the covariance 1/24 serve as quantitative indicators of the structural correlation between edges and faces.

These exact invariants are not only the theoretical foundation of this paper but also mathematical evidence that the geometry of the 600-cell contains an extremely precise algebraic structure. From Section III onward, upon this geometric foundation, the dynamic picture of vibrating force chains, the identity of time-averaging and renormalization, and the structure of six-hierarchy renormalization will be developed in sequence.

III. VIBRATING FORCE CHAINS AND THE DYNAMIC OPERATION OF THE SEPARATION DEVICE

A. Transition from the Static Picture to the Dynamic Picture

In Section II, the geometric attributes and the function as a separation device of the 600-cell were formulated statically. There, time-independent structures were described: the role division of the four attributes (vertex, edge, face, body), the closure of boundary surfaces, and the exact geometric invariants.

However, the actual operation of the separation device is a dynamic process involving temporal evolution. The topological residue δ is not a static quantity; as established in Section V.C of Part II, it is continuously generated and processed within an irreversible computational process. In this section, we introduce vibrating force chains as the physical implementation of this dynamic process and show that their temporal evolution constitutes the operation of the separation device.

B. The NP-hard Reconfiguration Problem and the Necessity of Vibration

In Section V.C of Part II, it was shown that the problem of packing regular tetrahedra in three-dimensional space is NP-complete. This computational complexity plays a decisive role in the dynamic picture of this paper.

For an NP-hard problem, a computational system cannot reach the complete solution (optimal packing, complete attainment of $\phi = \phi_c$) in finite time. The system continuously transitions among a set of approximate solutions, but the transition itself from one approximate solution to another generates new NP-hard subproblems. This process does not terminate.

Physically, this non-terminating computational process manifests as the continuous reconfiguration of force chain arrangements. A specific force chain configuration $\mathcal{F}_1$ at one instant t_1 transitions to another configuration $\mathcal{F}_2$ at the next instant t_2. The reconfiguration is computationally hard to predict deterministically, and to the observer it manifests as a probabilistic vibration.

An important point to emphasize is that the reconfiguration of force chains is not a disordered thermal fluctuation. Each instantaneous configuration $\mathcal{F}_n$ satisfies the geometric constraints (H_4 symmetry, coordination number 12, uniform cluster coefficient 5/11) as an approximate optimal solution at that point in time. The reconfiguration is a systematic process of transitioning within the space of approximate solutions while preserving these constraints.

C. Characteristic Time Scales of Vibration and the Necessity of the 10^6 Threshold

Let τ_n denote the characteristic time scale of vibration at each hierarchy n. The fundamental time unit at the lowest hierarchy (Planck scale) is the Planck time $t_P \approx 5.39 \times 10^{-44}$ s, which is the minimum update interval of the computational network established in Part II. The scale ratio between hierarchies is given as follows.

$$\tau_{n+1} = \tau_n \times 10^6, \qquad L_{n+1} = L_n \times 10^6 \tag{8}$$

The characteristic time scales of each hierarchy are shown in Table II.

The time scale ratio $\tau_{n+1}/\tau_n = L_{n+1}/L_n$ is a direct consequence of the Light-Speed Resource Allocation Principle $\tau_n = L_n/c$. However, why is the scale ratio 10^6 rather than some other value? The answer to this question is given from the thermodynamic perspective of the capacity limit of frustration.

a. Phase Transition Forced by the Capacity Limit of Frustration. A 10^6-fold increase in spatial scale implies a $(10^6)^3 = 10^{18}$-fold increase in volume. Inside the unit structure of hierarchy n, topological residue δ accumulates in proportion to its volume. Although the accumulation increases by a factor of 10^{18} with the scale-up, the geometric packing capacity of that hierarchy (the maximum amount of δ that can be confined internally through the closure of boundary surfaces) has a critical capacity specific to that hierarchy.

When the accumulated total of topological residue reaches this critical capacity, local processing at that hierarchy reaches its limit. At this point, the system has two options. The first is complete freezing (the asymptotic freezing discussed in Section III D), and the second is the phase transition to the upper hierarchy. Complete freezing halts temporal evolution and is inconsistent with the condition for the continued existence of the universe. Therefore the system necessarily selects the phase transition.

In this phase transition, the majority of the topological residue, now increased by a factor of 10^{18}, is reorganized as a single effective vertex of the upper hierarchy. The processing of the residue resumes at the operating point $\phi \approx 0.62$ of the newly formed upper hierarchy.

Therefore, the spatial scale ratio of 10^6 is not a coincidental value but appears as a critical condition under which the capacity limit of frustration forces a phase transition. The fact that the volume scale-up of 10^{18} is deeply connected with the geometric origin of the rigidity suppression ratio $\varepsilon_n \approx 10^{-19.2}$ at each hierarchy boundary will be discussed in detail in Section V.

The vibrating force chains at each hierarchy n reconfigure at the characteristic time scale τ_n. At time scales shorter than τ_n, the force chains appear static as a single configuration. At time scales longer than τ_n, an immense number of configurations are time-averaged, and traces of specific configurations disappear.

Hierarchy n	Physical identification	Spatial scale L_n (m)	Time scale τ_n (s)
0	Planck	10^{-35}	10^{-44}
1	QCD/hadron	10^{-15}	10^{-23}
2	Molecular	10^{-9}	10^{-17}
3	Cellular	10^{-3}	10^{-11}
4	Geological	10^{3}	10^{-5}
5	Planetary	10^{9}	10^{1}
6	Galactic	10^{21}	10^{13}

TABLE II. Characteristic spatial and temporal scales of the six hierarchies.

D. Asymptotic Freezing at the Operating Point $\phi \approx 0.62$

At each hierarchy, as the effective packing fraction ϕ approaches the jamming critical point $\phi_c \approx 0.64$, the reconfiguration of force chains asymptotically freezes. The divergence law of the reconfiguration time introduced in Section VI.B of Part II is reproduced here.

$$\tau_{\text{reconfig}} = \tau_0 \exp\left(\frac{E_0}{\phi_c - \phi}\right) \tag{9}$$

As $\phi \to \phi_c$, $\tau_{\text{reconfig}} \to \infty$, and the reconfiguration asymptotically halts.

The operating point of the universe $\phi \approx 0.62$ is located just before this divergence. Specifically, by maintaining a structural vacancy of $\phi_c - \phi \approx 0.02$, the finite value $\tau_{\text{reconfig}} \approx 12\, t_P$ is preserved. As a result, the reconfiguration of force chains continues at observable speeds, and the system avoids complete freezing.

The geometric origin of the structural vacancy $\phi_c - \phi \approx 0.02$ will be detailed in Section VII. In this section, we only record that this value is positioned as the condition that enables dynamic operation at the operating point.

E. The Dynamic Operation of the Separation Device and the Conservation of Frustration

The separation device introduced in Section II is reformulated in the dynamic picture of vibrating force chains. The input to the separation device is the total amount of unprocessed topological residue Φ_{in} arriving from the lower hierarchy. This input is sorted into three logically exclusive output paths through the passage of two geometric filters.

a. Two Geometric Filters. For the input topological residue, each regular tetrahedron (or its collection) faces two questions. The first question is the success or failure of projection: that is, of the four-dimensional structure, whether the relevant element is projected onto the three-dimensional observer's side. The answer to this question determines whether the element participates in three-dimensional geometric connection or remains on the four-dimensional side. The second question is the success or failure of structural fixation: that is, whether the element projected to the three-dimensional side is fixed as part of the rigidity network through the closure of boundary surfaces, or fails to be fixed and dissipates vibrationally. The answer to this question determines the amount of rigidity transmitted and the amount of heat dissipated.

Through the combination of these two filters, the input Φ_{in} branches into the following three output paths.

b. Path A (Projection ✓, Fixation ✓): Structural Stress. The portion that is projected to the three-dimensional side and is fixed as part of the rigidity network becomes structural stress transmitted to the upper hierarchy through the closure of boundary surfaces. This is the first output of the separation device, denoted as Φ_A.

c. Path B (Projection ✓, Fixation ×): Computational Entropy. The portion that is projected to the three-dimensional side but fails to be fixed due to vibration is dissipated as computational heat. According to Landauer's principle [4] established in Section V.C of Part II, each reconfiguration step generates a minimum heat of $k_B T \ln 2$. This heat is processed as dissipation to the lower hierarchy or as propagation to other parts within the same hierarchy. This is the second output of the separation device, denoted as Φ_B.

d. Path C (Projection ×): Unresolved Residue on the Four-Dimensional Side. The portion that fails to be projected to the three-dimensional side remains on the four-dimensional side. This is not directly observed by three-dimensional observers, but it is indirectly observed through gravitational effects. The "structure remaining on the four-dimensional side" anticipated in Section IV.A of Part I corresponds to this path and provides a geometric interpretation as a dark matter candidate. This is the third output of the separation device, denoted as Φ_C.

e. The Conservation of Frustration. The sum of these three outputs coincides with the total amount of the input topological residue.

$$\Phi_{\text{in}} = \Phi_A + \Phi_B + \Phi_C \tag{10}$$

This equation is formulated as the Conservation of Frustration. This is a dynamic version of the conservation of the total topological residue guaranteed by the Gauss–Bonnet theorem (Section IV.A of Part I), and it ensures that the operation of the separation device at each hierarchy boundary is described as a strict allocation process

of the universe's computational resources.

The combination of the two filters is logically exhaustive. The combination of the success or failure of projection (✓ or ×) and the success or failure of fixation (✓ or ×, where the latter is not asked in the case of projection ×) completely exhausts the three paths A, B, and C. Through this, the three-path output of the separation device is established not as a mere classification but as a necessary allocation based on a geometric conservation law.

The ratio of allocation to each path ($\Phi_A : \Phi_B : \Phi_C$) determines the operating characteristics of the separation device at each hierarchy. The specific structure of this ratio and its relation to the rigidity transmission ratio $\varepsilon_n \approx 10^{-19.2}$ at each hierarchy will be detailed in Section V.

F. Consistency between the Dynamic Picture and Isotropy

Here we confirm that the dynamic picture of vibrating force chains is consistent with the principles of isotropy and uniformity. In Section II F, the snapshot of volume ratios was computed with respect to a specific projection direction. In this computation, it was pointed out that the 600 regular tetrahedra are classified into 8 orbits, and which regular tetrahedron belongs to which orbit depends on the projection direction.

This projection-direction dependence appears to contradict isotropy as long as static snapshots are taken. However, in the dynamic picture of vibrating force chains, this apparent contradiction is resolved. At each instant, a specific force chain configuration $\mathcal{F}(t)$ has a specific directional character. However, the configurations continue to reconfigure, and all directions are statistically equally selected over the time scale of τ_n. Therefore, a system observed at time scales longer than τ_n exhibits a statistically isotropic structure.

This consequence establishes a central perspective of this paper. The observed isotropy emerges as the time-average of instantaneous directionalities. Isotropy is not a static property but a dynamic property achieved through the time-averaging of vibration. The identity of time-averaging and renormalization developed in Section IV is precisely a generalization of this observation.

G. Transition from a Single Computational Step to the Time Average

The snapshot of volume ratios $\langle (V_{3D}/V_{4D})^2 \rangle = 1/4$ introduced in Section II F should be precisely interpreted as an instantaneous value at a single computational step (the time scale of t_P). This instantaneous value gives the classification of 600 regular tetrahedra with respect to a specific projection direction. With respect to that direction, regular tetrahedra with volume ratio zero appear as 60 (one-tenth of the total), and regular tetrahedra with non-zero volume ratios appear as 540 (nine-tenths of the total).

However, this instantaneous value itself is not an observable physical quantity. Actual observation always has a finite time width $\tau_{\rm obs}$, and the time average over this time width becomes the observed quantity. In ordinary observations where $\tau_{\rm obs} \gg t_P$, an immense number of force chain configurations are averaged, and the instantaneous classification becomes meaningless to the observer.

Therefore, in this paper, the snapshot of volume ratios is positioned as a mathematical tool for describing the operation of the separation device at the minimum time unit. The observable physical consequences are described only through the time-averaging introduced in Section IV.

H. Summary of This Section

In this section, the transition from the static geometric foundation established in Section II to the dynamic picture of vibrating force chains was accomplished.

As the physical implementation of the NP-hard reconfiguration problem, force chain configurations continuously reconfigure. The characteristic time scale at each hierarchy n, $\tau_n = L_n/c$, is determined from the Light-Speed Resource Allocation Principle, and the ratio between adjacent hierarchies is 10^6. This value of 10^6 is not a coincidence but appears as a critical condition under which the capacity limit of frustration, associated with a volume ratio of 10^{18} in scale-up, forces a phase transition. The operating point $\phi \approx 0.62$, by maintaining the structural vacancy of $\phi_c - \phi \approx 0.02$ between itself and $\phi_c \approx 0.64$, avoids asymptotic freezing and maintains reconfiguration at observable speeds.

The separation device, through the combination of two geometric filters (the success or failure of projection and the success or failure of structural fixation), separates the input topological residue into three paths (structural stress, computational entropy, and unresolved residue on the four-dimensional side). The Conservation of Frustration, which states that the sum of these three outputs coincides with the input, is established as a dynamic version of the Gauss–Bonnet theorem. The projection-direction dependence is an instantaneous phenomenon, and statistical isotropy is achieved through averaging over the time scale of τ_n.

The snapshot of volume ratios $\langle (V_{3D}/V_{4D})^2 \rangle = 1/4$ is an instantaneous value at a single computational step, and observable physical quantities are defined only after time-averaging. The structure of this time-averaging will be described in Section IV in a unified manner with renormalization and scaling laws.

Figure 2. The Separation Device: Sequential Decomposition of Frustration

One input force is split by two binary filters — projection, then fixation — into three physical paths

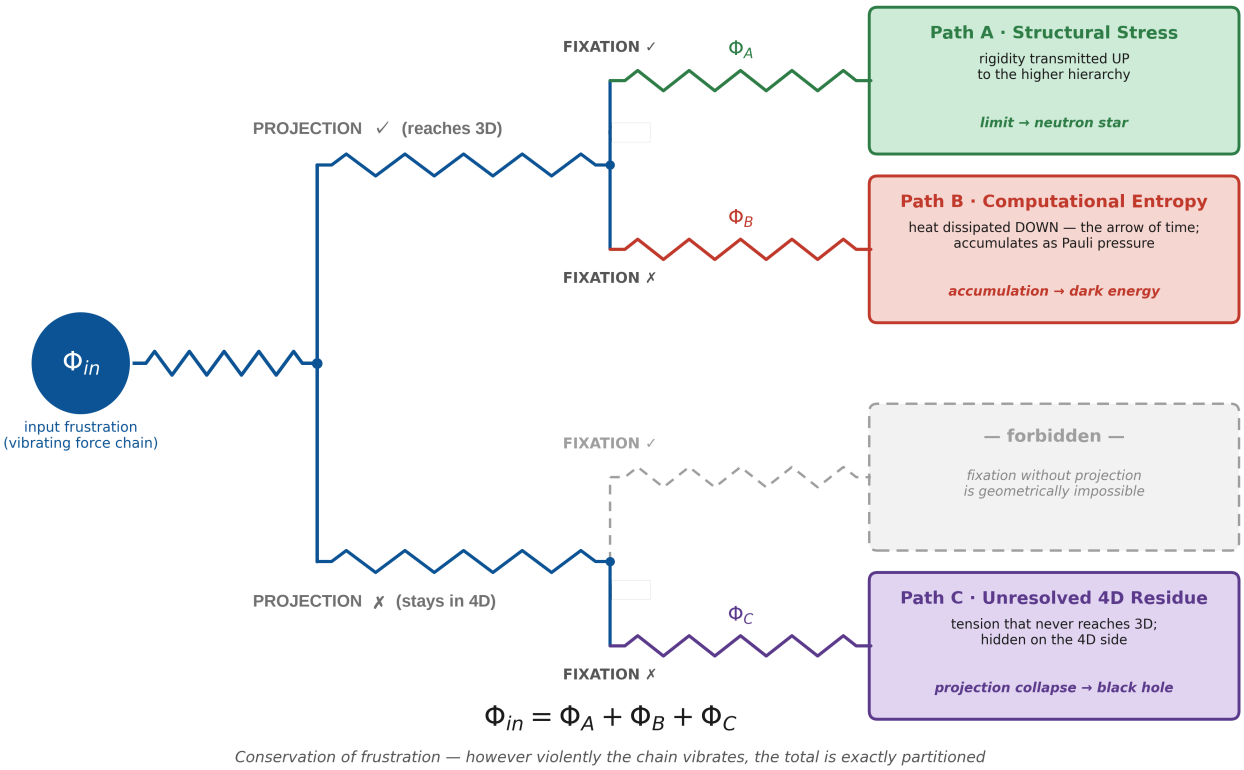

FIG. 2. **The Separation Device: Sequential Decomposition of Frustration.** One input force is split by two binary filters—projection, then fixation—into three physical paths. The input frustration Φ_{in} passes a projection filter (does it reach 3D?) and then a fixation filter (is it locked into the rigidity network?), yielding three mutually exclusive outputs: structural stress Φ_A (rigidity transmitted up; limit → neutron star), computational entropy Φ_B (heat dissipated down, the arrow of time; accumulates as dark energy), and unresolved 4D residue Φ_C (dark-matter candidate; projection collapse → black hole). The conservation law $\Phi_{\text{in}} = \Phi_A + \Phi_B + \Phi_C$ makes the partition exact, while fixation without projection is geometrically forbidden.

IV. THE IDENTITY OF TIME-AVERAGING AND RENORMALIZATION

A. The Central Claim of This Section

The central claim of this paper is expressed as the identity that the following four operations are different aspects of the same physical process. *Time-averaging, coarse-graining, renormalization, and scaling law—these four are the same operation.*

This identity is decomposed as follows. The operation of averaging the configurations of vibrating force chains at the lower hierarchy over the time scale τ (time-averaging) is equivalent to the operation of smoothing them spatially over the length scale $c\tau$ (coarse-graining). This operation directly functions as renormalization, which aggregates the lower-hierarchy degrees of freedom into the upper-hierarchy effective degrees of freedom, and as a consequence, the consistent rule across hierarchies is observed as a scaling law. In this section, this identity is established as a natural consequence of the Light-Speed Resource Allocation Principle $c^2 = v^2 + \tau^2$ from Part II.

B. The Observation Time Scale and the Observed Hierarchy

In Section III, the characteristic time scale of vibration τ_n at each hierarchy n was defined. Any observer has their own observation time scale τ_{obs}. The structure of the observed system is determined by the comparative relationship between this τ_{obs} and each τ_n. Specifically, in a system observed at the observation time scale τ_{obs}, the following three regimes are distinguished.

a. Regime 1: $\tau_{obs} \ll \tau_n$ (high-resolution regime). When the observation time scale is sufficiently shorter than the characteristic time scale of the relevant hierarchy, force chains appear as a static specific configuration. The observer sees a projection-direction-dependent structure at that instant.

b. Regime 2: $\tau_{obs} \approx \tau_n$ (resonant regime). When the observation time scale is comparable to the characteristic time scale of the relevant hierarchy, the reconfiguration of force chains appears to the observer as a significant dynamic process. The reconfiguration time τ_{reconfig} introduced in Section III.E of Part II corresponds to this time scale.

c. Regime 3: $\tau_{obs} \gg \tau_n$ (coarse-graining regime). When the observation time scale is sufficiently longer than the characteristic time scale of the relevant hierarchy, an immense number of force chain configurations are time-averaged. The observer cannot identify individual configurations and observes only statistical average values.

Actual physical observations typically lie in Regime 3 (the coarse-graining regime) with respect to a specific hierarchy's τ_n. For example, with respect to the galactic hierarchy $\tau_6 \approx 10^{13}$ s, cosmological observations occur at the time scale $\tau_{\text{obs}} \approx 10^{17}$ s (the age of the universe), achieving 10^4-fold coarse-graining. As a result, individual configurations of vibrating force chains at the galactic hierarchy are not observed; only the time-averaged statistical structure is observed.

C. The Principle that "Observation Time Determines the Object of Observation"

From the distinction of the three regimes in the previous subsection, an important methodological principle of this paper is derived.

Principle: The observation time scale determines the observed hierarchy.

Observations at different time scales are equivalent to observing different hierarchies. Short observation time scales capture the vibrational structures of lower hierarchies, while long observation time scales capture the stable structures of upper hierarchies. The two are not seeing different aspects of the same system but each takes its own hierarchy as the object of observation.

This principle provides a methodological guideline in cosmological observation. The composition of the universe (the ratios of dark matter, visible matter, and dark energy) is the structure at the largest hierarchy and is therefore a quantity determined by observation at the longest observation time scale (the age of the universe). Conversely, the composition at the QCD scale should be determined by observation at the characteristic time scale of that hierarchy; these are distinct quantities with different physical content.

This principle is understood as a natural extension into the time direction of the correspondence between observation wavelength and observation target in quantum mechanics ($\lambda = h/p$). In parallel with the way that short wavelengths (high energy) capture microscopic spatial structures, short observation times (high temporal resolution) capture the dynamic structures of lower hierarchies.

D. Mathematical Formulation of Time-Averaging

For a physical quantity $A(t)$, the time average over the time scale τ is defined as follows.

$$\langle A \rangle_\tau(t) = \frac{1}{\tau} \int_{t-\tau/2}^{t+\tau/2} A(t')\, dt' \tag{11}$$

For the force chain configuration $\mathcal{F}(t)$ defined in Section III, the time average $\langle \mathcal{F} \rangle_\tau$ is defined. In the case $\tau \gg \tau_n$, this time average is the statistical average of an immense number of configurations at hierarchy n.

The time-averaged configuration $\langle \mathcal{F} \rangle_{\tau_n}$ is qualitatively different from individual configurations $\mathcal{F}(t)$. Individual configurations are projection-direction-dependent and probabilistic, but time-averaged configurations are isotropic and deterministic. As established in Section III, isotropy is a dynamic property achieved through time-averaging.

E. Equivalence with Coarse-Graining

Time-averaging is equivalent to spatial coarse-graining. This equivalence is derived directly from the Light-Speed Resource Allocation Principle of Part II. The principle $c^2 = v^2 + \tau^2$ shows that the spatial degree of freedom v and the temporal degree of freedom τ share the same computational bandwidth c. Therefore, averaging by τ in the time direction is equivalent to treating a region extending by $c\tau$ in the spatial direction as a single unit.

Specifically, a quantity time-averaged at the observation time scale τ_{obs} corresponds to a quantity coarse-grained at the spatial scale $L_{\text{obs}} = c\,\tau_{\text{obs}}$. The relation $\tau_n = L_n/c$ for the characteristic time scale at hierarchy n is precisely an expression of this equivalence. Through this equivalence, time-averaging at the observation time scale automatically realizes coarse-graining at the corresponding spatial scale. The two are essentially two aspects of the same operation.

F. Time-Averaging as a Renormalization Operation

Having established the equivalence between time-averaging and coarse-graining, we now show that these function as a renormalization operation. A renormalization operation aggregates the lower-hierarchy degrees of freedom to constitute the upper-hierarchy effective degrees of freedom. The cooperative vibration of 100 effective vertices at hierarchy n ($\Omega_{\text{local}} = 100$, established in Part I), when averaged over the time scale τ_n, manifests as a single effective vertex at hierarchy $n+1$.

This aggregation is achieved by the details of vibration canceling each other out under time-averaging. The force chain configurations of 100 regular tetrahedra at the lower hierarchy continuously change at each instant,

but their average exhibits a stable macroscopic structure. This averaged structure functions as the position (vertex) of a computational node at the upper hierarchy.

The three-path output of the separation device established in Section III E is reinterpreted in the context of this renormalization operation. Path A (structural stress) is the path in which the vibration of the lower hierarchy is time-averaged and fixed as an effective vertex of the upper hierarchy. Path B (computational entropy) is the component canceled out in the averaging and dissipated as heat. Path C (residue on the four-dimensional side) is the component that does not participate in the projection to three dimensions in the first place.

The aggregation from 100 degrees of freedom at the lower hierarchy to 1 degree of freedom at the upper hierarchy is the contraction of information by the ratio $\Omega_{\text{local}} = 100$. Accompanying this contraction, the majority of the tension (the accumulation of topological residue) at the lower hierarchy is dissipated as heat, and only a small portion is preserved as the transmission of rigidity to the upper hierarchy. This preservation ratio is the rigidity transmission ratio $\varepsilon_n \approx 10^{-19.2}$ at each hierarchy.

G. Manifestation as Scaling Laws

The renormalization operation at each hierarchy boundary is a discontinuous phase transition. Each phase transition occurs independently of others, and different parameters (characteristic time scales, absolute values of structural stress, amounts of computational heat) appear at each hierarchy boundary.

However, a consistent rule persists across these phase transitions. At each hierarchy, the effective packing fraction $\phi \approx 0.62$ is universally observed, and the effective vertex count $\Omega_{\text{local}} \approx 100$ is reproduced. The topological residue $\delta \approx 7.36^\circ$ is preserved across all hierarchies.

This consistency arises from the fact that the renormalization operation at each hierarchy boundary is the same operation following the same geometry of the 600-cell. What differs across hierarchies is the parameter values; the structure of the renormalization operation itself does not depend on the hierarchy. This is the geometric origin of scaling laws. The observed scaling law is the manifestation of the invariance of the renormalization operation across hierarchies.

H. The Coexistence of Discontinuity and Consistency

Integrating the discussion thus far, the answer is obtained to the question posed at the beginning of this paper—the existence of a consistent rule across discontinuous phase transitions.

The origin of discontinuity lies in the fact that the renormalization operation at each hierarchy boundary occurs as a discrete jump. The transition from the degrees of freedom at hierarchy n to those at hierarchy $n+1$ is not a continuous deformation but occurs at once as aggregation by the ratio $\Omega_{\text{local}} = 100$.

The origin of consistency lies in the fact that the renormalization operation at each hierarchy boundary follows the same geometric structure (the 600-cell). Even when the hierarchy changes, the operation applied is isomorphic, and the resulting rules are also isomorphic.

The two are not contradictory. Discontinuous phase transitions are the discrete manifestations of a consistent operation. Each phase transition is not an independent event but a recurrence of the same operation at each hierarchy boundary.

When this perspective is visualized, the central claim of this paper is expressed as follows. In the three-dimensional time-averaging tunnel defined by the Light-Speed Resource Allocation Principle $c^2 = v^2 + \tau^2$, the state of the observation target changes its position discretely as the hierarchy ascends. The three axes of this tunnel are constructed with the X-axis as the observation time scale (hierarchy n), the Y-axis as the spatial fluctuation v, and the Z-axis as the temporal stability τ. All cross-sections in the Y–Z plane are constrained to the half-arc $v^2 + \tau^2 = c^2$ defined by the Light-Speed Resource Allocation Principle. That is, the entire tunnel is unfolded in three-dimensional space as the roof of a half-cylinder.

The trajectory of the observation target proceeds within this tunnel from the far side of the X-axis (lowest hierarchy) toward the near side (highest hierarchy). At the lowest hierarchy, the trajectory oscillates with large amplitude in the Y-axis direction (high spatial fluctuation v) while remaining at a low position in the Z-axis direction (low temporal stability τ). As the observation time scale grows larger (proceeding toward the near side of the X-axis), time-averaging cancels out the oscillations in the Y-axis direction, and the Y-axis width of the trajectory contracts. Accompanying the contraction of the Y-axis width, the trajectory necessarily ascends in the Z-axis direction due to the constraint of the roof of the half-cylinder. At the highest hierarchy, the trajectory reaches the top of the half-cylinder ($v \approx 0$, $\tau \approx c$).

This ascending process is not continuous but occurs as discrete jumps at each hierarchy boundary. Within a hierarchy, the trajectory proceeds approximately parallel to the Y-axis, but when the capacity limit of frustration is reached, a discrete transition to the next hierarchy occurs, and the trajectory jumps in a staircase pattern in the Z-axis direction. However, all jumps occur within the same three-dimensional tunnel, and the cross-section in the Y–Z plane is always constrained to the same half-arc $v^2 + \tau^2 = c^2$. This is the visual expression of how a consistent geometric rule is maintained across discontinuous phase transitions.

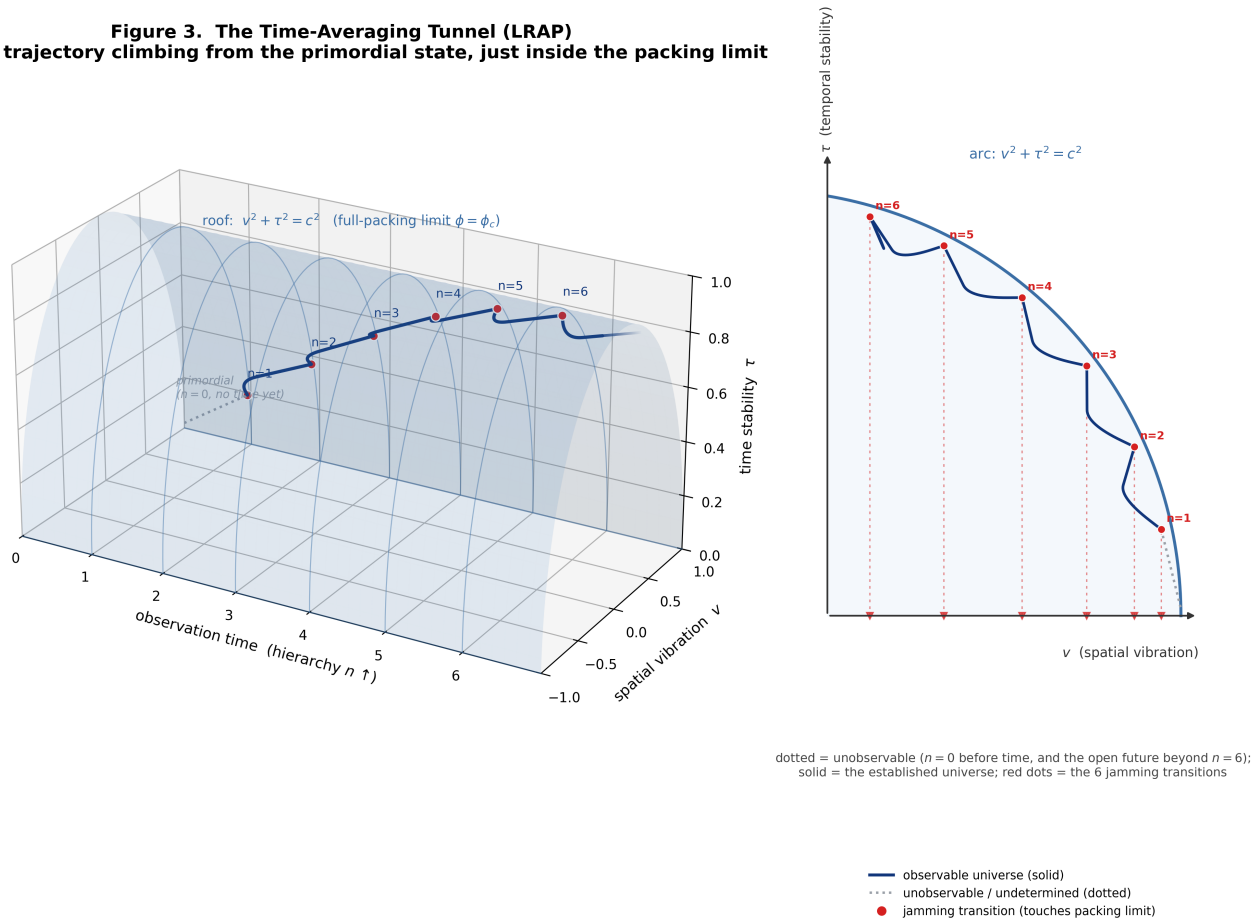

FIG. 3. **The Time-Averaging Tunnel (LRAP).** A single trajectory climbing from the primordial state, just inside the packing limit. Inside the half-cylinder roof $v^2 + \tau^2 = c^2$ (the full-packing limit $\phi = \phi_c$), one continuous trajectory climbs the observational hierarchy $n = 1 \to 6$, as spatial vibration v is time-averaged away and temporal stability τ rises; each ramp accumulates frustration until it touches the limit at a jamming transition (red dot) and then snaps inward to renormalize. Solid marks the established, observable universe; the dotted primordial lead-in ($n = 0$) and the fade beyond $n = 6$ mark the unobservable past and the undetermined future.

I. The Universe as an "Observational Staircase"

Based on the discussion in the previous subsection, the hierarchical structure of the universe is redescribed as follows. The universe is not a continuous spacetime but an observational staircase consisting of six steps. Each step has its own characteristic time scale τ_n and spatial scale $L_n = c\tau_n$, and the structure of that hierarchy is determined by observation at that time scale. The observer sees structures at a height of the staircase corresponding to their own observation time scale.

The transition from a lower step to an upper step is not continuous but occurs as a discrete 10^6-fold time scale jump and 10^{18}-fold volume scale jump. At each transition, the 100 degrees of freedom at the lower hierarchy are reorganized as a single degree of freedom at the upper hierarchy. This reorganization necessarily occurs as the phase transition forced by the capacity limit of frustration (Section III).

The transmission ratio of rigidity at each step is $\varepsilon_n \approx 10^{-19.2}$, and the cumulative ratio through six steps is $\varepsilon_{\text{total}} \approx 10^{-115.2}$. That the suppression by this accumulation is consistent with the observed cosmological constant problem (a discrepancy of 122 orders of magnitude) will be detailed in Section V.

J. Summary of This Section

In this section, the central claim of this paper was established. The identity that time-averaging, coarse-graining, renormalization, and scaling law are the same operation is derived as a natural consequence of the Light-Speed Resource Allocation Principle of Part II.

The principle that the observation time scale determines the observed hierarchy was established. Different observation time scales take different hierarchies as objects of observation. The composition of the universe is a

quantity determined at the longest observation time scale (the age of the universe).

Through the mathematical formulation of time-averaging, it was shown that the time average of vibrating force chain configurations emerges as an isotropic and deterministic structure. The equivalence with coarse-graining is derived directly from the Light-Speed Resource Allocation Principle, and averaging in the time direction corresponds to coarse-graining in the spatial direction.

Time-averaging as a renormalization operation aggregates the 100 degrees of freedom at the lower hierarchy into 1 degree of freedom at the upper hierarchy. The contraction of information accompanying this aggregation is the origin of the rigidity transmission ratio $\varepsilon_n \approx 10^{-19.2}$ at each hierarchy.

The coexistence of discontinuous phase transitions and consistent rules is not a contradiction but is understood as the discrete manifestations of the same renormalization operation. The hierarchical structure of the universe is redescribed as an "observational staircase" consisting of six steps. In Section V, the structure of renormalization operations established in this section is quantitatively developed, and the approach to the cosmological constant problem as the accumulation of six hierarchies is discussed.

V. THE QUANTITATIVE STRUCTURE OF SIX-HIERARCHY RENORMALIZATION AND THE COSMOLOGICAL CONSTANT PROBLEM

A. The Scope of This Section

In Section IV, the identity of time-averaging, coarse-graining, renormalization, and scaling law was established. The renormalization operation at each hierarchy boundary aggregates the $\Omega_{\text{local}} = 100$ degrees of freedom at the lower hierarchy into a single effective degree of freedom at the upper hierarchy. In this section, this renormalization operation is quantitatively developed, and the cumulative structure across six hierarchies is described.

Specifically, this section addresses the structure of the rigidity transmission ratio ε_n at each hierarchy, its cumulative result $\varepsilon_{\text{total}}$ over six hierarchies, and the demonstration that this accumulation is consistent with the observed cosmological constant problem (a discrepancy of 122 orders of magnitude).

However, an important caveat must be noted regarding this section. The first-principles derivation of the specific numerical value $\varepsilon_n \approx 10^{-19.2}$ has not been completed within the scope of this paper. The complete connection between the exact geometric invariants presented in Section II ($\langle \sin^4 \theta_e \rangle = 5/8$, the proportional relation 2/3 between edges and faces, the covariance 1/24, and others) and this specific numerical value remains as a subject for future research. This section explicitly records this incompleteness and develops, with intellectual honesty, the scope that can be presented at the present time.

B. The Rigidity Transmission Ratio at a Single Hierarchy

The separation device established in Section III E separates the input topological residue into three paths (Path A: structural stress, Path B: computational entropy, Path C: unresolved residue on the four-dimensional side). The Conservation of Frustration $\Phi_{\text{in}} = \Phi_A + \Phi_B + \Phi_C$ holds. The rigidity transmission ratio ε_n at hierarchy n is defined as the ratio of Path A to the input.

$$\varepsilon_n = \frac{\Phi_A^{(n)}}{\Phi_{\text{in}}^{(n)}} \tag{12}$$

That is, it represents the fraction of the topological residue arriving at a given hierarchy that is transmitted as rigidity to the upper hierarchy. As a numerical characteristic of this ratio, the following value is required by inverse calculation from the observed cosmological constant problem.

$$\varepsilon_n \approx 10^{-19.2} \tag{13}$$

Several candidates have emerged regarding the geometric origin of this value. As the first candidate, the exact geometric invariant $\langle \sin^4 \theta_e \rangle = 5/8$ established in Section II F is noted. This value is a rational number in the immediate vicinity of the operating point $\phi \approx 0.62$ and strongly suggests the geometric origin of the jamming critical point ϕ_c. Computing $\phi_c^{\Omega_{\text{local}}} = (5/8)^{100}$ yields approximately $10^{-20.4}$. This differs from the observed value $10^{-19.2}$ by 1.2 orders of magnitude—close, but not a complete match.

As the second candidate, using the empirical critical point $\phi_c \approx 0.64$ from jamming physics, $0.64^{100} \approx 10^{-19.4}$ is obtained. This value is extremely close to the observed value, but $\phi_c = 0.64$ is an empirical value that has not been derived from first principles within the framework of this paper.

As the third candidate, there exists a composite indicator constructed from the proportional relation 2/3 between edges and faces and the covariance 1/24 established in Section II. The specific formulation of ε_n from these quantities has not yet been established at the present time.

To select the correct first principle from among these candidates, further refinement of the physical mechanism governing the operation of the separation device is necessary. In this paper, we proceed with the value $\varepsilon_n \approx 10^{-19.2}$ as given, and explicitly identify its first-principles derivation as a subject for future research.

Figure 4. The Observational Staircase

Six discrete hierarchies, each set by its own observation time — yet every step runs the same renormalization

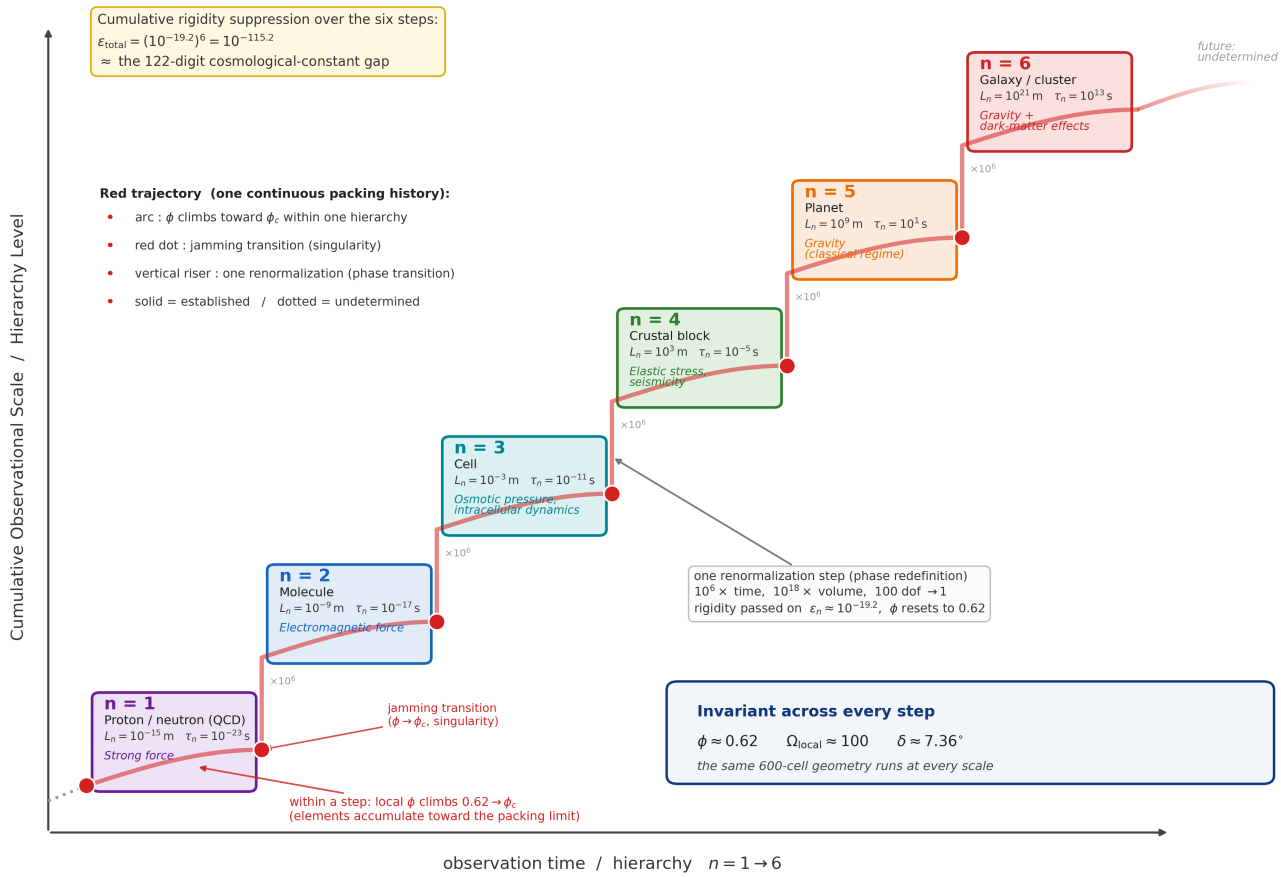

FIG. 4. **The Observational Staircase.** Six discrete hierarchies, each set by its own observation time—yet every step runs the same renormalization. The universe is redrawn as six discrete steps climbing in cumulative scale: within each step the local packing fraction ϕ rises from the operating point ≈ 0.62 toward ϕ_c, a jamming transition (red dot) occurs, and a vertical riser renormalizes ~ 100 degrees of freedom into one ($\times 10^6$ in time, $\times 10^{18}$ in volume) while passing on rigidity $\varepsilon_n \approx 10^{-19.2}$. Across six steps the cumulative suppression $\varepsilon_{\text{total}} \approx 10^{-115.2}$ approaches the 122-digit cosmological-constant gap, even though $\phi \approx 0.62$, $\Omega_{\text{local}} \approx 100$ and $\delta \approx 7.36°$ remain invariant at every scale.

C. The Geometric Position of the Structural Vacancy 0.02

The difference between the operating point $\phi \approx 0.62$ and the critical point $\phi_c \approx 0.64$, $\phi_c - \phi \approx 0.02$, was introduced in Section III D as the "structural vacancy." Within the framework of this paper, this value simultaneously fulfills the following three roles. First, the avoidance of asymptotic freezing: by keeping ϕ at the operating point without reaching ϕ_c, the divergence of the reconfiguration time $\tau_{\text{reconfig}} \to \infty$ is avoided. Second, the dynamic maintenance of renormalization operations: through the continuation of the reconfiguration of force chains at finite speeds, the renormalization operation at each hierarchy boundary operates continuously. Third, the function as the leak path of force: in the concept of boundary surfaces introduced in Section II, the structural vacancy functions as the leak path through which forces (the observed physical interactions) manifest.

Considering these roles, $\phi_c - \phi \approx 0.02$ is not merely a numerical error but an essential geometric margin necessary for the dynamic operation of the universe. The difference 0.015 between $5/8 = 0.625$ presented in Section II and the empirical critical point 0.64 is understood as one quantitative indicator of this structural vacancy. However, the geometric necessity for the value of this margin to be specifically 0.02 has not been completely established within the scope of this paper. This is also recorded as a subject for future research.

D. Accumulation across Six Hierarchies

As established in Section III, the spatial scale ratio 10^6 appears as the critical condition under which the capacity limit of frustration forces a phase transition. The six-hierarchy structure is formed as this critical condition is repeated six times. When the rigidity transmission ratio $\varepsilon_n \approx 10^{-19.2}$ at each hierarchy boundary is accumulated across hierarchies, the cumulative ratio after six hierarchies is as follows.

$$\varepsilon_{\text{total}} = \prod_{n=1}^{6} \varepsilon_n \approx (10^{-19.2})^6 = 10^{-115.2} \tag{14}$$

Since the transmission of rigidity at each hierarchy is a probabilistic and irreversible process, the accumulation operates multiplicatively. This is the geometric version of the chain rule in information theory.

E. Physical Identification of the Six Hierarchies

Each hierarchy is characterized by its characteristic time scale τ_n and spatial scale L_n, and possesses corresponding physical units. We reproduce Table II from Section III and add the physical phenomena dominantly observed at each hierarchy (Table III).

At each hierarchy, the physical phenomena characteristic of that hierarchy are observed. Within the framework of this paper, all of these phenomena are manifestations of the same renormalization operation at different scales. The forces observed become weaker as the hierarchy ascends, and the transition from the strong force (hierarchy 1) to gravity (hierarchy 6) is the physical expression of the cumulative suppression $\varepsilon_{\text{total}} \approx 10^{-115.2}$.

Between the lowest and highest hierarchies, there is a 36-order-of-magnitude difference in spatial scale (10^{-15} to 10^{21}), which is consistent with the strength difference of the observed forces (the ratio of the strong force to gravity, $\sim 10^{38}$). This consistency is qualitative evidence that the framework of this paper correctly captures the physical hierarchical structure.

F. Approach to the Cosmological Constant Problem

In quantum field theory, the theoretical estimate of the vacuum energy density includes divergent terms at the Planck scale, and its ratio to the observed cosmological constant Λ_{obs} reaches the following order [5].

$$\frac{\rho_{\text{vacuum, theoretical}}}{\rho_{\text{vacuum, observed}}} \sim 10^{122} \tag{15}$$

This is known as the "cosmological constant problem" and is one of the largest unsolved problems in modern physics.

Within the framework of this paper, this 122-order-of-magnitude discrepancy is understood as a natural consequence of cumulative suppression through hierarchical renormalization. The vacuum energy at the Planck scale (hierarchy 0) is suppressed by the ratio $\varepsilon_{\text{total}} \approx 10^{-115.2}$ by the time it reaches the galactic hierarchy (hierarchy 6) after passing through six hierarchies of renormalization.

This value does not completely match the observed 122-order suppression, leaving a discrepancy of 6 orders of magnitude. This discrepancy is considered to consist of the following two contributions. First, the contribution of Path C (unresolved residue on the four-dimensional side). In the Conservation of Frustration $\Phi_{\text{in}} = \Phi_A + \Phi_B + \Phi_C$, Path C is not directly observed by three-dimensional observers. When this is observed as dark matter, its quantity functions as an additional suppression with respect to Path A (structural stress). Second, additional partial suppressions within each hierarchy. Before reaching the boundary of each hierarchy, there also exists local dissipation within that hierarchy. The total of these contributions is conjectured to constitute the additional suppression of approximately 7 orders of magnitude from $10^{-115.2}$ to 10^{-122}.

The precise quantification of these additional suppressions is a subject for future research beyond the scope of this paper. What is established in this paper is the qualitative and order-of-magnitude correspondence that the cumulative structure of six hierarchies provides a quantity consistent with the observed 122-order suppression.

G. The Composition of the Universe and the Observation Time Scale

According to the methodological guideline established in Section IV C—the observation time scale determines the observed hierarchy—the composition of the universe (the ratios of dark matter, visible matter, and dark energy) is a quantity determined by observation at the longest observation time scale (the age of the universe, $\sim 10^{17}$ s). The observed values in modern cosmology [8] are given as follows.

- Visible matter: approximately 5%
- Dark matter: approximately 27%
- Dark energy: approximately 68%

Within the framework of this paper, these values are interpreted as follows. Visible matter is observed as the accumulation of Path A (the component transmitted to the upper hierarchy as structural stress). The rigidity that reaches the three-dimensional observer after passing through six hierarchies of renormalization appears as visible matter. Dark matter is observed as the accumulation of Path C (unresolved residue on the four-dimensional side). It is a structure that is not projected into three

Hierarchy n	Scale L_n (m)	Unit structure	Major observed phenomenon
1	10^{-15}	Proton/neutron (QCD)	Strong force
2	10^{-9}	Molecule	Electromagnetic force
3	10^{-3}	Cell	Osmotic pressure, intracellular dynamics
4	10^{3}	Crustal block	Elastic stress, seismicity
5	10^{9}	Planet	Gravity (classical regime)
6	10^{21}	Galaxy, galaxy cluster	Gravity + dark matter effects

TABLE III. Physical identification of the six hierarchies and their dominant observed phenomena.

dimensions but is indirectly observed through gravitational effects. The "structure remaining on the four-dimensional side" anticipated in Section IV.A of Part I corresponds to this. Dark energy is observed as the accumulation of Path B (computational entropy dissipated as heat). As discussed in Section IV F, the contraction of information accompanying renormalization is dissipated as heat. This dissipation has no equilibrium partner and continues to accumulate throughout the universe. This is the origin of the observed accelerated expansion [6, 7].

The perspective that the cumulative ratios of Paths A, B, and C correspond to the composition of the universe (5%, 27%, 68%) is a qualitative prediction derived naturally from the framework of this paper. Specific quantification (for example, "why is dark matter precisely 27% rather than 30%?") requires precise calculation of the path-branching ratios at each hierarchy and is beyond the scope of this paper.

H. The Current Status of Zero-Parameter Derivation

Within the framework of this paper, the quantities that have been established with zero free parameters and those that remain unestablished at the present time are organized as follows.

a. Quantities established with zero free parameters (already derived in Parts I, II, and Section II of this paper):

- Topological residue $\delta = 2\pi - 5\arccos(1/3) \approx 7.36^\circ$ (Niven's theorem)
- Effective vertex count $\Omega_{\text{local}} \approx 100$ (H_4 symmetry)
- Gravitational constant G (1.1% agreement with observed values)
- Exact geometric invariants $\langle \sin^2\theta_e \rangle = 3/4$, $\langle \sin^2\theta_{\text{face}} \rangle = 1/2$, $\langle \sin^4\theta_e \rangle = 5/8$, and others
- Inter-hierarchy scale ratio $L_{n+1}/L_n = 10^6$ (necessity from the capacity limit of frustration)
- Number of hierarchies $N = 6$ (logical consequence of Section III)

b. Quantities unestablished at the present time (subjects for future research):

- First-principles derivation of the rigidity transmission ratio $\varepsilon_n \approx 10^{-19.2}$ at each hierarchy
- Geometric necessity of the structural vacancy $\phi_c - \phi \approx 0.02$
- Quantification of the path-branching ratios for Paths A, B, and C
- Quantitative prediction of the composition of the universe (5%, 27%, 68%)

To achieve complete zero-parameter status, first-principles derivations of the unestablished quantities are necessary. This paper, as an intermediate stage toward this ultimate goal, develops the framework that can be presented at the present time with intellectual honesty, explicitly distinguishing between the established and unestablished portions.

I. Summary of This Section

In this section, the quantitative structure of six-hierarchy renormalization was developed. The rigidity transmission ratio $\varepsilon_n \approx 10^{-19.2}$ at each hierarchy accumulates across six hierarchies and yields a suppression ratio $\varepsilon_{\text{total}} \approx 10^{-115.2}$. This value exhibits an order of magnitude consistent with the observed cosmological constant problem (a discrepancy of 122 orders of magnitude). The remaining discrepancy of approximately 7 orders of magnitude is understood as the contribution of Path C (a dark matter candidate) and the accumulation of local dissipation within each hierarchy.

The physical identification of the six hierarchies corresponds to the scale hierarchy of QCD, molecular, cellular, geological, planetary, and galactic, and the forces observed at each hierarchy (the strong force, electromagnetic force, osmotic pressure, elastic stress, classical gravity, and galactic-hierarchy gravity) are manifestations of the same renormalization operation at different scales.

The composition of the universe (visible matter 5%, dark matter 27%, dark energy 68%) is interpreted as the accumulation of the three paths of the separation device (Paths A, B, and C). This is a qualitative prediction derived naturally from the framework of this paper.

Regarding the current status of zero-parameter derivation, the established and unestablished quantities were explicitly distinguished. The first-principles derivation of $\varepsilon_n \approx 10^{-19.2}$, the geometric necessity of the structural vacancy 0.02, and the quantification of the path-branching ratios all remain as subjects for future research. In Section VI, the scope of applications suggested by the framework of this paper is presented as a broad overview across scales.

VI. THE SCOPE OF APPLICATIONS

A. The Approach of This Section

Through Section V, the theoretical core of this paper (the 600-cell as a separation device, the identity of time-averaging and renormalization, the cumulative structure across six hierarchies) has been established. In this section, we present a broad overview of the applications suggested by this framework, ranging from the quantum scale to the cosmological scale.

For each application, what this paper provides is not "a complete explanation of the phenomenon" but "a new perspective for capturing the phenomenon." Specific quantitative predictions and technical applications are positioned as future research subjects in each respective specialized field. The purpose of this section is to show that the framework of this paper is not a theory limited to a specific scale but provides a universal perspective applicable across hierarchies.

B. Quantum Scale: Strong Coupling and Nucleon Arrangement

At hierarchy 1 (QCD/hadron scale, $L_1 \approx 10^{-15}$ m) in Table III, the strong force is observed as the dominant physical phenomenon. Within the framework of this paper, the strong force is understood as the geometric tension at the boundary surfaces of protons and neutrons (the local concentration points of the topological residue δ).

As discussed in Section II, the closure cost at each hierarchy decreases as the hierarchy ascends. At the QCD scale, near the lowest hierarchy, the closure cost of the boundary surfaces of unit structures (protons) is maximal, which manifests as the extremely high coupling constant $\alpha_s \sim 0.1$ of the strong force.

Physical phenomena related to nucleon arrangement (nuclear fusion, nuclear fission, the stability of atomic nuclei) are redescribed within the framework of this paper as problems of geometric connection between the boundary surfaces of protons and neutrons. When multiple nucleons are arranged in close proximity, the geometric connection of their boundary surfaces achieves partial local resolution of the topological residue. The geometric details of this resolution are a subject for future research beyond the scope of this paper.

C. Molecular Scale: Protein Tertiary Structure

At hierarchy 2 (molecular scale, $L_2 \approx 10^{-9}$ m), the electromagnetic force is observed as the dominant physical phenomenon. Among the characteristic structure formations at this hierarchy, the tertiary structure formation of biopolymers (particularly the folding of proteins) is noteworthy.

Protein folding is a process in which a linear amino acid chain spontaneously reorganizes into a three-dimensional tertiary structure. Within the framework of this paper, this reorganization is understood as a kind of jamming transition. The amino acid chain does not freely move through a continuous conformational space; rather, it undergoes discrete structural transitions in accordance with the cooperative rigidity network formation with $\Omega_{\text{local}} = 100$ established in this paper.

The recent success of structure prediction by machine learning (such as AlphaFold) suggests that the structural space of proteins is not disordered but possesses some geometric regularity. The framework of this paper proposes a discrete structure based on regular tetrahedra as the origin of this regularity. Specific verification (geometric analysis of the internal representations of machine learning models) is a subject for future research.

D. Cellular Scale: Cytoplasmic Jamming

The cytoplasm at hierarchy 3 (cellular scale, $L_3 \approx 10^{-3}$ m) has been shown by recent research to function near the operating point of jamming transitions [10]. The observed effective packing fraction of cytoplasm is approximately $\phi \approx 0.62$, consistent with the operating point presented in this paper.

Within the framework of this paper, the fact that cytoplasm functions at the jamming operating point is not a coincidence but is understood as the manifestation at the cellular scale of geometric conditions that hold universally at each hierarchy. The dynamic processes within cells (protein transport, cell division, morphological changes) are redescribed as the reconfiguration of vibrating force chains near the operating point. This perspective opens the possibility of directly connecting cellular dynamics research in biophysics with the framework of this paper.

E. Geological Scale: Earthquake Dynamics

Earthquake phenomena at hierarchy 4 (geological scale, $L_4 \approx 10^3$ m) have already been discussed in detail in an independent paper based on the framework of this paper [16]. In that companion paper, it was shown that

the framework of this paper provides new perspectives on the following seismological problems: the physical origin of the P-wave to S-wave velocity ratio, the geometric derivation of the parameters of the Rate-and-State friction law, the reinterpretation of deep earthquakes as four-dimensional junction failures, and the generation mechanism of large-scale earthquakes through lubricated criticality. Detailed discussion at the geological scale is left to that companion paper.

F. Planetary and Galactic Scales: Gravity and Dark Matter

At hierarchy 5 (planetary scale, $L_5 \approx 10^9$ m) and hierarchy 6 (galactic scale, $L_6 \approx 10^{21}$ m), gravity is observed as the dominant physical phenomenon. Within the framework of this paper, gravity is understood as the closure cost of boundary surfaces after reaching the uppermost hierarchies. As discussed in Section V, due to the cumulative suppression of six hierarchies, $\varepsilon_{\text{total}} \approx 10^{-115.2}$, the coupling constant at the galactic hierarchy (corresponding to the gravitational constant G) takes an extremely small value.

The dark matter effects observed at the galactic hierarchy are interpreted, as discussed in Section V G, as the accumulation of Path C (unresolved residue on the four-dimensional side) of the separation device. At the uppermost hierarchy, the inhomogeneous distribution of rigidity may become prominent. That is, within galactic halos, regions where the rigidity network is completed on the four-dimensional side (not observed by three-dimensional observers but possessing gravitational effects) and regions where the connection between four dimensions and three dimensions is complete (observed as visible matter) may coexist. The geometric details of this rigidity inhomogeneity are a subject for future research beyond the scope of this paper.

G. Implications for Quantum Information Processing

The framework of this paper may provide a new perspective on the fundamental problems of quantum information processing (particularly quantum computation). The central technical challenge in quantum computation is the maintenance of coherence. Within the framework of this paper, coherence is reinterpreted as an unpacked state (a state in which the boundary surface has not been eliminated and the continuity with four dimensions is preserved). Decoherence is understood as the local progression of the natural tendency of the universe (the closure of boundary surfaces toward the saving of frustration-processing costs).

At the lower hierarchy, the reconfiguration of force chains proceeds at the characteristic time scale τ_{QCD}. Quantum computation systems implement operations that proceed with computation while avoiding determination (the completion of packing, i.e., decoherence) against this dynamic state space. This is an operation that runs counter to the natural tendency of the universe, and it inherently involves time limitations.

From this perspective, the essence of quantum computation lies in the dynamic control of the boundary between the continuous unpacked state and the discrete determined state. The relationship between the divergent exploration of state space and the convergence at the necessary moment (measurement) is parallel to the structure of hierarchical renormalization discussed in this paper. Implications for specific technological applications are beyond the scope of this paper, but it is worth pointing out the possibility that this perspective may serve as a starting point for reconsidering the geometric foundations of quantum information processing.[19]

H. Cosmological Scale: Cosmological Constant and Composition Ratios

At cosmological scales beyond hierarchy 6 ($L \gtrsim 10^{26}$ m, the cosmological horizon scale), the cosmological constant Λ_{obs} and the composition of the universe (visible matter 5%, dark matter 27%, dark energy 68%) are observed as physical quantities. As discussed in Sections V F and V G, within the framework of this paper, the cosmological constant problem (a 122-order-of-magnitude discrepancy) is understood as a natural consequence of cumulative suppression through hierarchical renormalization, and the composition of the universe is interpreted as the accumulation of the three paths of the separation device (Paths A, B, and C).

These interpretations show that the framework of this paper yields orders of magnitude consistent with cosmological observations. Specific quantitative predictions (for example, the first-principles derivation that "dark energy is precisely 68%") require precise calculation of the path-branching ratios at each hierarchy and are beyond the scope of this paper.

I. A Transverse Perspective: Consistency across Hierarchies

The applications presented thus far are all specific physical phenomena at specific hierarchies. However, the most important contribution of the framework of this paper lies in the fact that these phenomena are understood in a unified manner as manifestations of the same renormalization operation at different scales.

The strong force (QCD scale), the electromagnetic force (molecular scale), cellular dynamics (cellular scale), earthquakes (geological scale), gravity (planetary and galactic scales), and the cosmological constant (cosmological scale)—these have traditionally been studied as independent physical phenomena, but within the frame-

work of this paper, they share the geometry of the 600-cell as a common origin.

The universality of the operating point $\phi \approx 0.62$ at each scale, the cross-hierarchical reproducibility of the effective vertex count $\Omega_{\text{local}} \approx 100$, and the preservation of the topological residue $\delta \approx 7.36^\circ$ are all different aspects of the invariance of the renormalization operation across hierarchies. This transverse perspective opens the possibility of reconsidering, under a unified geometric framework, phenomena that have traditionally been studied in different academic disciplines. Within the scope of this paper, it is not possible to develop each application in depth, but further verification and development by specialists in each field is anticipated.

J. Summary of This Section

In this section, applications suggested by the framework of this paper were presented as a broad overview, ranging from the quantum scale to the cosmological scale. Each application (strong coupling, protein folding, cytoplasmic jamming, earthquake dynamics, gravity and dark matter, quantum information processing, the cosmological constant) is redescribed from a new perspective within the framework of this paper. Specific quantitative predictions and technical applications are positioned as future research subjects in each respective specialized field.

The transverse significance of these applications lies in the fact that physical phenomena that have traditionally been studied independently share the geometry of the 600-cell as a common origin. The invariance of the renormalization operation across hierarchies is observed as the universal operating point $\phi \approx 0.62$ and the effective vertex count $\Omega_{\text{local}} \approx 100$ at each scale. In Section VII, the most fundamental dynamic property of the framework of this paper—the stability at the operating point $\phi \approx 0.62$—is discussed.

VII. THE STABILITY OF THE OPERATING POINT $\phi \approx 0.62$ AND THE BOUNDARY DEFINITION OF LIFE

A. The Scope of This Section

In Section V, the structural vacancy $\phi_c - \phi \approx 0.02$ between the operating point $\phi \approx 0.62$ and the critical point $\phi_c \approx 0.64$ was positioned as an essential geometric margin necessary for the dynamic operation of the universe. In this section, the stability of this operating point is analyzed more deeply, and its physical and geometric consequences are developed.

Specifically, we discuss the following: that the operating point is characterized as a dynamic trajectory proceeding along the inside of the arc; that this trajectory is understood as the balance between gravity (structural stress) and Pauli repulsion (the pressure of computational entropy); that life is defined as a system located at the boundary of this operating point; and that rigidity inhomogeneity at the uppermost hierarchy may serve as the geometric origin of the observed cosmic structure.

B. The Dynamic Trajectory of the Operating Point: The Inside of the Arc

In Section IV, it was discussed that the state of the universe is represented as a point on the half-arc defined by the Light-Speed Resource Allocation Principle $c^2 = v^2 + \tau^2$. The renormalization operation at each hierarchy boundary manifests as discrete positional changes on this half-arc.

However, an important refinement is necessary in this picture. The actual state of the universe is not strictly located on the half-arc, but proceeds at a position slightly displaced inward from the half-arc. The magnitude of this displacement corresponds to the structural vacancy $\phi_c - \phi \approx 0.02$.

The half-arc itself represents the complete packing limit ($\phi = \phi_c$, the point at which phase transitions occur). At the moment of reaching this limit, the divergence of the reconfiguration time $\tau_{\text{reconfig}} \to \infty$ occurs, and the system asymptotically freezes. The actual universe never reaches this limit and continues to proceed along its inside.

This dynamic trajectory proceeds along the time direction in parallel with the arc within each hierarchy, and at the point where the capacity limit of frustration is reached, it jumps to the next hierarchy. Between hierarchy-boundary jumps, the trajectory progressively ascends along the inside of the arc, with the vibration amplitude v gradually decreasing and the temporal stability τ increasing.

This picture provides a dynamic refinement of the "observational staircase" introduced in Section IV. Each step of the staircase is not a perfect horizontal line but a spiral trajectory with a slight upward inclination. Within each step, the system continues to accumulate frustration, and at the point where the capacity limit is reached, a discrete jump to the next step occurs.

C. The Dynamic Balance between Gravity and Pauli Repulsion

The mechanism by which the operating point is maintained on the inside of the half-arc is understood as the balance of two opposing forces.

a. Gravity (structural stress). As the accumulation of the closure cost of boundary surfaces introduced in Section II, gravity acts in the direction of compressing the unit structures at each hierarchy. This manifests as the observed gravitational field. Gravity acts to push the operating point up toward the half-arc.

b. Pauli repulsion (the pressure of computational entropy). As established in Axiom Zero in Part I, the "real existence at zero distance" of quantum entanglement and the "prohibition of the same location" of the exclusion principle are two faces of the same mathematical fact. This exclusivity acts as computational entropy, as a pressure that continues to accumulate throughout the universe. Pauli repulsion acts to push the operating point away from the half-arc and inward.

The equilibrium point of the two is the observed operating point $\phi \approx 0.62$. This equilibrium is not static but dynamic. Compression by gravity and counter-pressure by Pauli repulsion offset each other moment by moment, and the system continues to proceed along the inside of the half-arc in the time direction.

As established in Part II, the accelerated expansion of the universe (dark energy) is the manifestation of the cumulative pressure of Pauli repulsion. While gravity achieves local equilibrium, Pauli repulsion has no equilibrium partner and continues to accumulate throughout the universe. This asymmetry is the origin of the observed accelerated expansion.

D. The Triple Role of the Structural Vacancy 0.02

As anticipated in Section V, the structural vacancy $\phi_c - \phi \approx 0.02$ plays a triple role in the dynamic operation of the universe. In this section, these roles are developed in an integrated manner.

a. First role: the avoidance of asymptotic freezing. By keeping ϕ at the operating point without reaching ϕ_c, the divergence of the reconfiguration time is avoided. The reconfiguration of force chains continues at finite speeds, and the temporal evolution of the universe is maintained.

b. Second role: the dynamic maintenance of renormalization operations. The renormalization operation at each hierarchy boundary operates through the continuation of force chain reconfiguration. In the state of complete freezing, renormalization halts, and the maintenance of the hierarchical structure becomes impossible. The structural vacancy is an essential condition for dynamically maintaining the renormalization operation.

c. Third role: the function as the leak path of force. In the concept of boundary surfaces introduced in Section II, the structural vacancy functions as the path through which internal frustration leaks to the outside. This leakage is the origin of the observed physical interactions (the strong force, electromagnetic force, gravity, and others). In the state of complete packing, the boundary surface is completely closed, and the propagation of force to the outside halts.

These three roles are not independent of each other but are different aspects of the same geometric margin. The operating point $\phi \approx 0.62$ is the unique geometric position at which these three roles are simultaneously fulfilled. The difference 0.015 between the exact geometric invariant $\langle \sin^4 \theta_e \rangle = 5/8 = 0.625$ presented in Section II F and the empirical critical point $\phi_c \approx 0.64$ from jamming physics is one quantitative indicator of this structural vacancy. The fact that the difference between them is neither 0 nor greater than 0.02 suggests that the geometric position of the operating point is determined with extreme precision.

E. The Dynamic Stability near the Operating Point

The operating point $\phi \approx 0.62$ is not merely an equilibrium point but possesses dynamic stability against perturbations. When ϕ moves slightly from the operating point toward the ϕ_c side, the reconfiguration time τ_{reconfig} rapidly increases. As a result, the responsiveness of the system decreases, and the accumulation of frustration accelerates. When the accumulated frustration exceeds the capacity limit, a phase transition is triggered, and renormalization to the upper hierarchy occurs. This process acts to push the system back to the operating point.

Conversely, when ϕ moves slightly from the operating point to a lower value, the reconfiguration of force chains becomes excessively fast, and the formation of the rigidity network becomes insufficient. As a result, the transmission of structural stress decreases, and the counterforce of gravity against Pauli repulsion weakens. The system is again compressed and returns to the operating point.

Through this dynamic stability, the operating point $\phi \approx 0.62$ is maintained as the long-term operational condition of the entire universe. The structural stability of the observed universe (the long lifespans of stars, the long-term maintenance of galaxies) is understood as a manifestation of the dynamic stability of this operating point.

F. The Boundary Definition of Life

In Section VI.E of Part I, the boundary definition of life was anticipated: that life is a system located at the boundary between structural stress (gravity, rigidity) and computational entropy (heat, Pauli repulsion). In this section, this definition is refined within the framework of this paper.

a. Life as the operating point. Life is a system that functions near the operating point $\phi \approx 0.62$. This fact is observationally supported by the fact mentioned in Section VI that the effective packing fraction of cytoplasm is $\phi \approx 0.62$. Life functions at the same position as the operating point of the entire universe.

b. Life as a dynamic boundary. Life is characterized as a system that dynamically maintains the operating point. Non-living systems can also function at the operating point, but they are limited to passive responses to perturbations. Life, through active processes (metabolism, self-organization), continuously corrects deviations from the operating point. This active-

ness has a structure parallel to "the dynamic preservation of the unpacked state" discussed in Section VI. Life, at the boundary between structural stress and computational entropy, does not completely succumb to either and continues to maintain a dynamic equilibrium.

c. The three quantitative conditions of life. Within the framework of this paper, the boundary definition of life is expressed as the following three quantitative conditions. First condition: functioning near the operating point, $\phi \approx 0.62$ (more specifically, maintaining the structural vacancy $\phi_c - \phi \approx 0.02$). Second condition: positive generation rate of structural entropy, $dS_{\text{struct}}/dt > 0$; life actively maintains the formation of the rigidity network, preventing collapse into disordered dissipation. Third condition: the scale of the cooperative rigidity network, $\langle Z \rangle \geq 3$, where Z is the cooperative coordination number among the constituent elements of the system, and $Z \geq 3$ corresponds to the geometric minimum condition for the formation of the rigidity network. A system that simultaneously satisfies these three conditions is the geometric definition of life within the framework of this paper.

G. The Asymmetry of Computational Entropy and the Flow of Time

As discussed above, a fundamental asymmetry exists between gravity (structural stress) and Pauli repulsion (computational entropy). Gravity achieves local equilibrium, while computational entropy has no equilibrium partner and continues to accumulate throughout the universe. Within the framework of this paper, this asymmetry is positioned as the origin of the flow of time.

The renormalization operation at each hierarchy aggregates the vibrating force chains of the lower hierarchy into the stable structure of the upper hierarchy. Accompanying this aggregation, computational entropy is dissipated as Path B to the lower hierarchy. The dissipated entropy is partially processed within the lower hierarchy, but complete resolution is not achieved. The residual entropy continues to accumulate throughout the universe.

This accumulation process is the observed irreversible flow of time. The origins of the three irreversibilities discussed in Section V.C of Part II (the cost of information erasure, computational complexity, and the one-directionality of projection) are all different aspects of this asymmetric accumulation of computational entropy. Life is positioned as a boundary system that locally processes a portion of this asymmetric accumulation process. The metabolism of life is the local dissipation of computational entropy, and through this dissipation, life dynamically maintains the boundary between structural stress and computational entropy.

H. Rigidity Inhomogeneity at the Uppermost Hierarchy

The behavior of the operating point at the uppermost hierarchy (hierarchy 6, galactic scale) may exhibit characteristic structures different from those at lower hierarchies. At lower hierarchies, the boundary surfaces of each unit structure close locally within the hierarchy. Through this closure, the internal frustration is locally confined, and leakage to the outside is limited to gradual processes through the structural vacancy.

At the uppermost hierarchy, this local closure may not be completely achieved. At the galactic scale, since there is no longer a destination for renormalization to a higher hierarchy, the accumulation of frustration must be processed within the hierarchy. However, this processing capacity also has limits, and as a result, spatial inhomogeneity in the rigidity network may occur.

Specifically, within the uppermost hierarchy, regions where the rigidity network is completed on the four-dimensional side (not observed by three-dimensional observers but possessing gravitational effects) and regions where the connection between four dimensions and three dimensions is complete (observed as visible matter) may coexist. This rigidity inhomogeneity is positioned as a geometric origin candidate of the observed dark matter effects. This picture is consistent with the interpretation as the accumulation of Path C (unresolved residue on the four-dimensional side) discussed in Section V G. The rigidity inhomogeneity at the uppermost hierarchy is understood as the result of Path C accumulating in a spatially biased form.

However, the geometric details of this rigidity inhomogeneity (specific spatial distribution, temporal evolution, correspondence with observed galactic structures) are subjects for future research beyond the scope of this paper. In this section, this prediction is recorded as a direction toward future refinement.

I. The Operating Point and the Condition for the Continued Existence of the Universe

The stability of the operating point developed in this section functions as the condition for the long-term continued existence of the universe. If the universe were to deviate from the operating point and reach the state of complete packing ($\phi = \phi_c$), temporal evolution would halt due to asymptotic freezing. In this case, the universe would freeze on an infinite time scale, and physical activity for the observer would come to an end.

Conversely, if the universe were to deviate from the operating point and reach a sufficiently low packing fraction, the formation of the rigidity network would become impossible. In this case, the transmission of structural stress would halt, and the stability of matter (stars, galaxies, the constituent elements of life) would collapse.

The fact that the observed universe continues to exist

in the long term is evidence that the dynamic stability of the operating point has been maintained over a long period. Within the framework of this paper, this maintenance is explained as a natural geometric condition (a consequence of Axiom Zero). The stability of the operating point is not the result of special initial conditions or fine-tuning of the universe but is a necessity naturally derived from the geometry of the 600-cell.

J. Summary of This Section

In this section, the stability of the operating point $\phi \approx 0.62$ was deeply analyzed within the framework of this paper. The operating point was characterized as a dynamic trajectory proceeding along the inside of the half-arc (the complete packing limit defined by the Light-Speed Resource Allocation Principle). This inward displacement corresponds to the structural vacancy $\phi_c - \phi \approx 0.02$. The maintenance of the operating point is understood as the dynamic balance between gravity (structural stress) and Pauli repulsion (computational entropy).

The structural vacancy simultaneously fulfills three roles (the avoidance of asymptotic freezing, the dynamic maintenance of renormalization operations, and the function as the leak path of force). These three roles are different aspects of the same geometric margin. The vicinity of the operating point possesses dynamic stability against perturbations and is maintained as the long-term operational condition of the entire universe.

Life is defined as a system located at the boundary of the operating point, satisfying three quantitative conditions (functioning near the operating point, the positive generation rate of structural entropy, and the formation of the cooperative rigidity network). Life is a boundary system that actively maintains the boundary between structural stress and computational entropy, and locally processes a portion of the asymmetric accumulation of computational entropy.

Rigidity inhomogeneity at the uppermost hierarchy was positioned as a geometric origin candidate of the observed dark matter effects. A detailed geometric description of this rigidity inhomogeneity is a subject for future research. The dynamic stability of the operating point is the long-term condition for the continued existence of the universe and is a necessity naturally derived from the geometry of the 600-cell. In Section VIII, the discussion of this paper is integrated, and the significance of the entire trilogy and the scope of future research are presented.

VIII. CONCLUSIONS AND FUTURE PROSPECTS

A. The Main Achievements of This Paper

As the concluding part of the Regular Simplex Hierarchical Gravity (RSHG) trilogy, this paper has constructed the theory of hierarchical renormalization. Following the static geometry of Part I (the derivation from Axiom Zero to the gravitational constant G) and the dynamics of Part II (the Light-Speed Resource Allocation Principle, the resolution of singularities), this paper has established the thermodynamic structure. The main achievements are organized as follows.

First, the completion of the geometric attributes of the 600-cell. The body (three-dimensional cell) was added as the fourth attribute to the three attributes (vertices, edges, faces) established up to Part II, and was positioned as the unit of rigidity and the container of the topological residue δ. Through this, the role of the 600-cell was completely described in two stages: as a transducer (Parts I and II) and as a separation device (this paper).

Second, the establishment of new exact geometric invariants. $\langle \sin^2 \theta_{\text{face}} \rangle = 1/2$ is a new exact invariant for faces, on par with $\langle \sin^2 \theta_{\text{edge}} \rangle = 3/4$ for edges. $\langle \sin^4 \theta_e \rangle = 5/8$, the proportional relation 2/3 between edges and faces, and the covariance 1/24 were also established as exact rational numbers. These constitute mathematical evidence that the H_4 symmetry of the 600-cell contains an extremely precise algebraic structure.

Third, the establishment of the identity of time-averaging and renormalization. The central claim that time-averaging, coarse-graining, renormalization, and scaling law are different aspects of the same physical process was derived as a natural consequence of the Light-Speed Resource Allocation Principle $c^2 = v^2 + \tau^2$. The methodological guideline that the observation time scale determines the observed hierarchy was established.

Fourth, the formulation of the Conservation of Frustration. The three-path output of the separation device (Path A: structural stress, Path B: computational entropy, Path C: unresolved residue on the four-dimensional side) was logically derived from the combination of two geometric filters (the success or failure of projection, the success or failure of structural fixation), and $\Phi_{\text{in}} = \Phi_A + \Phi_B + \Phi_C$ was established as a dynamic version of the Gauss–Bonnet theorem.

Fifth, the quantitative structure of six-hierarchy renormalization. The spatial scale ratio of 10^6 was made necessary as the phase transition forced by the capacity limit of frustration, and the cumulative ratio across six hierarchies $\varepsilon_{\text{total}} \approx 10^{-115.2}$ was shown to provide an order of magnitude consistent with the observed cosmological constant problem (a discrepancy of 122 orders of magnitude).

Sixth, the dynamic stability of the operating point $\phi \approx 0.62$. The operating point was characterized as a dynamic trajectory proceeding along the inside of the

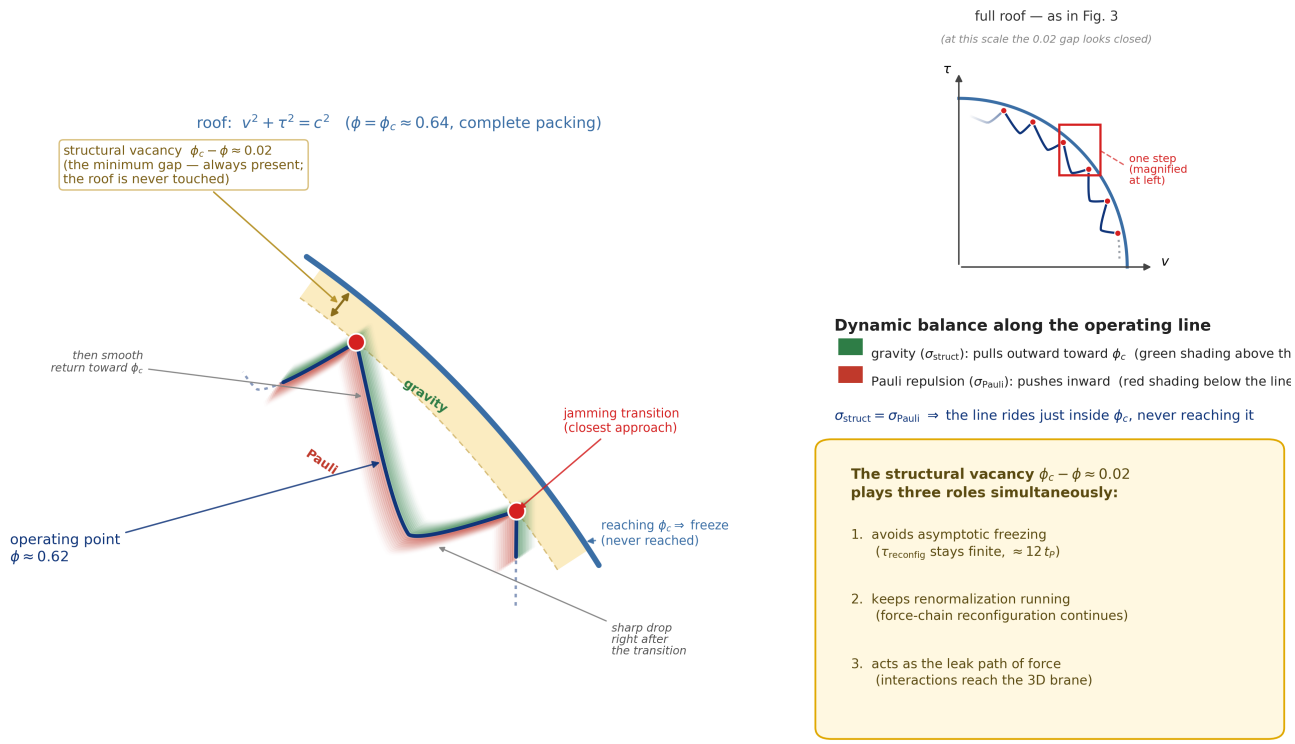

FIG. 5. **Spiral Dynamic Trajectory near the Operating Point.** One hierarchical step, from one jamming transition to the next—the operating line never touches the roof; a structural vacancy $\phi_c - \phi \approx 0.02$ always remains. Magnifying a single step of Figure 3, the operating line rides the balance between gravity (structural stress, green, pulling outward toward ϕ_c) and Pauli repulsion (computational entropy, red, pushing inward), so that even at its closest approach—the jamming transition—it stays a finite structural vacancy $\phi_c - \phi \approx 0.02$ short of the limit and never reaches it. That residual vacancy plays three simultaneous roles: averting asymptotic freezing, sustaining the renormalization dynamics, and serving as the leak path through which forces reach the 3D brane.

complete packing limit, and it was shown that the structural vacancy $\phi_c - \phi \approx 0.02$ simultaneously fulfills three roles (the avoidance of asymptotic freezing, the dynamic maintenance of renormalization, and the function as the leak path of force). Life was defined, with three quantitative conditions, as a system located at the boundary of this operating point.

B. The Integration of the Trilogy: From Axiom Zero to Hierarchical Renormalization

Throughout the entire trilogy, RSHG theory has been developed as a framework that describes a wide range of physical phenomena in a unified manner from a single starting point (Axiom Zero).

Axiom Zero: Quantum entanglement and the exclusion principle are two faces of the same mathematical fact—the impossibility of filling three-dimensional space with regular tetrahedra. This identity is naturally derived from the topological residue $\delta = 2\pi - 5\arccos(1/3)$ established as an algebraic necessity through Niven's theorem.

Part I (static geometry): Starting from Axiom Zero, the 600-cell as the escape route into four dimensions was geometrically derived as a necessity, and the effective vertex count $\Omega_{\text{local}} \approx 100$ was derived with zero free parameters. Through this, the 1.1% agreement with the observed gravitational constant G was achieved.

Part II (dynamics): Dynamics were constructed on the static geometry. The Light-Speed Resource Allocation Principle $c^2 = v^2 + \tau^2$ was established as the bandwidth allocation of the computational network, and the origins of mass, force, and time were geometrically redescribed. Singularities were reinterpreted as dimensional arrest.

This paper (thermodynamics): Hierarchical structure was constructed on the dynamics. By time-averaging functioning as renormalization, the six-hierarchy struc-

ture of the universe is necessarily formed. The dynamic stability of the operating point $\phi \approx 0.62$ at each hierarchy guarantees the long-term continued existence of the universe.

The logical structure of the trilogy is integrated as a triple development from Axiom Zero. The 600-cell functions as a transducer (from four-dimensional tension to three-dimensional force) in Part I and as a separation device (from frustration into structural stress and computational entropy) in this paper. Both functions are two aspects derived from the same geometry. The dynamic structures established throughout Parts II and this paper (the flow of time, the asymmetric accumulation of computational entropy, the boundary definition of life) are all consequences naturally derived from Axiom Zero.

C. The Geometric Origin of Quantum Entanglement

Axiom Zero positioned quantum entanglement as an observed fact at the starting point of the trilogy. Through the development of the trilogy, the possibility has been shown that quantum entanglement can be geometrically reinterpreted within the framework of this paper.

Path C (unresolved residue on the four-dimensional side) of the separation device established in Section III E describes structures that are not projected to three dimensions but are connected four-dimensionally. The dynamic preservation of the unpacked state discussed in Section VI has a structure parallel to the maintenance of coherence in quantum information processing.

Synthesizing these, quantum entanglement may be reinterpreted as follows. When two particles spatially separated in three dimensions are in quantum entanglement, they exist as two three-dimensional projections of a single structure that has not yet been four-dimensionally separated. To three-dimensional observers, they appear as "two separated particles," but on the four-dimensional side, separation has not been completed (packing is incomplete). The observation (completion of packing) of one particle instantaneously determines the state of the other particle through the four-dimensional continuity.

This picture can develop in parallel with the standard description of quantum information theory (the off-diagonal elements of the density matrix, the violation of Bell inequalities), and the establishment of the precise correspondence between the two is an important subject for future research.

The phenomenon that, even though the unpacked state persists at the microscopic scale, only the determined classical states are observed at the macroscopic scale, is explained within the framework of this paper as the difference in observation time scales. At macroscopic observation time scales, individual configurations of microscopic vibrating force chains are averaged out and become invisible, and only the determined averaged structures are observed. The phenomenon "even though things overlap and are entangled at the microscopic scale, no problem arises at the macroscopic scale" is a natural consequence of the central claim of this paper—that the observation time scale selectively observes the corresponding hierarchy.

D. Subjects for Future Research

Several important unsolved problems remain within the framework of this paper. These suggest natural directions for the development of the trilogy.

First, the first-principles derivation of the rigidity transmission ratio $\varepsilon_n \approx 10^{-19.2}$. In this paper, this value was described based on inverse calculation from observed values and partial consistency with geometric invariants. The specific formulation that completely derives ε_n from the exact geometric invariants established in Section II ($\langle \sin^4 \theta_e \rangle = 5/8$, the proportional relation 2/3 between edges and faces, the covariance 1/24) has not been established. This is the most important subject for completing the logic of the trilogy.

Second, the geometric necessity of the structural vacancy $\phi_c - \phi \approx 0.02$. The first-principles derivation that the difference between the operating point and the critical point is precisely this value has not been established. The refinement of the relationship with the difference 0.015 between 5/8 and the empirical critical point 0.64 is necessary.

Third, the geometric details of the rigidity inhomogeneity at the uppermost hierarchy. As anticipated in Section VII, the spatial distribution of the rigidity network at the galactic hierarchy becomes a geometric origin candidate of the observed dark matter distribution and dark matter effects. Specific formulations (such as the four-dimensional bubble structure model) have a scope to be developed in independent future papers.

Fourth, the geometric description of intelligence. The concept of the dynamic preservation of the unpacked state anticipated in Section VI has the possibility of developing, at a point beyond the scope of this paper, into a physical definition of "intelligence." The opposing structures of divergence and convergence, continuity and discreteness, and determination and indeterminacy are candidates for fundamental concepts describing the essence of intelligence. This is a subject to be developed as an independent research program after the completion of the trilogy.

Fifth, specific verification in each field of application. Specific quantitative predictions and experimental verification in each application example mentioned in Section VI (strong coupling at the quantum scale, protein structure, cellular dynamics, quantum information processing, and others) are subjects for future research requiring collaboration with specialists in each field.

E. The Path toward Zero-Parameter Status

Throughout the trilogy, the ideal of zero-parameter status has been pursued in stages. The derivation of the gravitational constant G in Part I was a partial realization achieving 1.1% agreement with observed values. In this paper as well, multiple quantities including $\Omega_{\text{local}} \approx 100$, the number of hierarchies $N = 6$, and the inter-hierarchy scale ratio 10^6 have been established with zero free parameters.

However, quantities that have not yet reached first-principles derivation also exist, such as $\varepsilon_n \approx 10^{-19.2}$, the structural vacancy 0.02, and the composition of the universe. The existence of these unestablished portions indicates that the trilogy is not the final theory of physics but a theory under construction. This paper, by explicitly distinguishing between the established and unestablished portions, has maintained an attitude of intellectual honesty. This transparency enables verification by reviewers and clarifies the path toward future development. The achievement of complete zero-parameter status is a goal to be pursued through future research as a natural development of the trilogy.

F. Relationship with Existing Physics

The framework of this paper does not negate existing physics but reconstructs it on a deeper geometric foundation.

a. Relationship with quantum mechanics. As established in Part II, special relativity is derived as a theorem from the Light-Speed Resource Allocation Principle. The hierarchical renormalization of this paper provides a bridge between the probabilistic description of quantum mechanics and the deterministic description of classical physics. Depending on the observation time scale, microscopic quantum fluctuations and macroscopic classical stability appear as different aspects of the same system.

b. Relationship with general relativity. In Part I, the gravitational constant G was geometrically derived. The framework of this paper redescribes gravity as the closure cost of boundary surfaces at the uppermost hierarchy. The continuous spacetime description of general relativity is positioned as the coarse-grained limit of the discrete computational network of this paper.

c. Relationship with statistical mechanics and thermodynamics. The asymmetric accumulation of computational entropy established in this paper provides the geometric origin of the second law. Information thermodynamics (Landauer's principle) is naturally integrated within the framework of this paper.

d. Relationship with jamming physics. Empirical concepts of jamming physics, such as the operating point $\phi \approx 0.62$, the critical point $\phi_c \approx 0.64$, and the critical exponent $\nu \approx 0.88$, are redescribed as geometric necessities in this paper. Research in granular physics and glass transitions is positioned as the venue for specific experimental verification within the framework of this paper.

e. Relationship with causal dynamical triangulations. Causal dynamical triangulations (CDT) recover a macroscopic four-dimensional de Sitter geometry as an emergent, statistical outcome of summing over discrete causal geometries [11–13]. The framework of this paper suggests a complementary reading, in which a static, highly symmetric skeleton—here the 600-cell $\{3, 3, 5\}$—may act as an attractor underlying that emergent geometry, so that what CDT reaches dynamically and what this paper posits as a primary structure could be two descriptions of the same fixed point. Whether the operating point $\phi \approx 0.62$ and the invariants $\delta \approx 7.36°$, $\Omega_{\text{local}} \approx 100$ admit a quantitative match to CDT observables is left as an open question.

f. Relationship with the thermal time hypothesis. The treatment of time in this paper—as the downward dissipation of frustration, i.e. computational entropy, and the asymmetric accumulation discussed in Section VII G—resonates with the thermal time hypothesis of Connes and Rovelli [14, 15], in which the flow of time is not fundamental but is fixed by the thermodynamic state of the system. In that language, the identity of time-averaging and renormalization established in Section IV may be read as selecting, at each hierarchy, the modular flow appropriate to the thermal state of that scale. We record this only as a possible point of contact; making the correspondence precise is a subject for future research.

These relationships with existing physics show that RSHG theory functions not as an independent alternative theory but as a unified redescription of existing physics.

G. Concluding Remarks

At the end of the trilogy, we reconfirm the fundamental perspective of this paper. The universe is a computational process that naturally unfolds from a single algebraic fact—the impossibility of filling three-dimensional space with regular tetrahedra. This computational process does not complete; rather, it continuously refines itself through an infinite hierarchical structure. Each hierarchy has its own time scale and spatial scale, generating its own physical units (protons, molecules, cells, crustal rocks, planets, galaxies).

The renormalization operation that crosses hierarchies aggregates the vibrating force chains of the lower hierarchy into the stable structure of the upper hierarchy. Accompanying this aggregation, the input topological residue is separated into three paths: structural stress (transmitted upward as rigidity), computational entropy (dissipated downward as heat), and unresolved residue on the four-dimensional side (remaining as gravitational effects). The Conservation of Frustration ensures that these separations are strictly preserved as the geometric budget allocation of the entire universe.

The dynamic balance between gravity and Pauli repulsion at the operating point $\phi \approx 0.62$ is the natural geometric condition guaranteeing the long-term continued existence of the universe. As a system located at the boundary of this balance, life is quantitatively defined. Life actively maintains the boundary between structural stress and computational entropy and locally processes a portion of the asymmetric accumulation of computational entropy.

The framework of this paper provides a unified perspective that crosses physics, biology, information science, and cosmology. It has been shown that groups of phenomena that have developed independently in their respective fields share the geometry of the 600-cell as a common origin. This unification is the main contribution of the trilogy and simultaneously a starting point for new approaches to unsolved problems.

The logic of the trilogy, beginning from Axiom Zero and reaching the structure of hierarchical renormalization, here sees one form of completion. However, the groups of unsolved problems (the first-principles derivation of ε_n, the geometric description of intelligence, the precise formulation of quantum entanglement, and others) indicate that this completion is not the end point but a new starting point. The true verification and development of RSHG theory begin from here.

ACKNOWLEDGMENTS

This work was carried out as independent research, without institutional affiliation or external funding. The author thanks Claude (Anthropic) and Gemini (Google DeepMind) for assistance with drafting, translation, figure preparation, and cross-checking throughout the trilogy.

[1] I. Niven, *Irrational Numbers*, Carus Mathematical Monographs No. 11 (Mathematical Association of America, Washington, D.C., 1956).
[2] A. J. Liu and S. R. Nagel, Jamming is not just cool any more, *Nature* **396**, 21 (1998).
[3] C. S. O'Hern, L. E. Silbert, A. J. Liu, and S. R. Nagel, Jamming at zero temperature and zero applied stress: The epitome of disorder, *Phys. Rev. E* **68**, 011306 (2003).
[4] R. Landauer, Irreversibility and heat generation in the computing process, *IBM J. Res. Dev.* **5**, 183 (1961).
[5] S. Weinberg, The cosmological constant problem, *Rev. Mod. Phys.* **61**, 1 (1989).
[6] A. G. Riess *et al.* (High-z Supernova Search Team), Observational evidence from supernovae for an accelerating universe and a cosmological constant, *Astron. J.* **116**, 1009 (1998).
[7] S. Perlmutter *et al.* (Supernova Cosmology Project), Measurements of Ω and Λ from 42 high-redshift supernovae, *Astrophys. J.* **517**, 565 (1999).
[8] Planck Collaboration, Planck 2018 results. VI. Cosmological parameters, *Astron. Astrophys.* **641**, A6 (2020).
[9] H. Furstenberg and I. Tzkoni, Spherical functions and integral geometry, *Israel J. Math.* **10**, 327 (1971).
[10] T. E. Angelini, E. Hannezo, X. Trepat, M. Marquez, J. J. Fredberg, and D. A. Weitz, Glass-like dynamics of collective cell migration, *Proc. Natl. Acad. Sci. U.S.A.* **108**, 4714 (2011).
[11] J. Ambjørn, J. Jurkiewicz, and R. Loll, Emergence of a 4D world from causal quantum gravity, *Phys. Rev. Lett.* **93**, 131301 (2004).
[12] J. Ambjørn, J. Jurkiewicz, and R. Loll, Reconstructing the universe, *Phys. Rev. D* **72**, 064014 (2005).
[13] J. Ambjørn, A. Görlich, J. Jurkiewicz, and R. Loll, Nonperturbative quantum gravity, *Phys. Rep.* **519**, 127 (2012).
[14] A. Connes and C. Rovelli, Von Neumann algebra automorphisms and time-thermodynamics relation in generally covariant quantum theories, *Class. Quantum Grav.* **11**, 2899 (1994).
[15] C. Rovelli, Statistical mechanics of gravity and the thermodynamical origin of time, *Class. Quantum Grav.* **10**, 1549 (1993).
[16] R. Sato, Crustal Jamming Dynamics (in preparation, 2026).
[17] The higher moments $\langle \cos^{2k} \theta_e \rangle$ are expected to possess a recursive structure with respect to k. Values such as $\langle \cos^6 \theta_e \rangle = 5/64$ and $\langle \cos^8 \theta_e \rangle = 7/128$ are derived as exact rational numbers. A complete algebraic analysis of these values is beyond the scope of this paper and remains as a subject for future research.
[18] Of the six orbits, 180 faces have $\sin^2 \theta_{\text{face}} = (3-\sqrt{5})/6 = 1/(3\phi^2)$, and another 180 faces have $\sin^2 \theta_{\text{face}} = (3+\sqrt{5})/6 = \phi^2/3$. In these two orbits, the $\sqrt{5}$ terms cancel out symmetrically. (Here ϕ denotes the golden ratio.)
[19] The perspective of reformulating the maintenance of coherence as "the dynamic preservation of the unpacked state" has room to develop in parallel with the standard description of quantum information theory (described as the preservation of off-diagonal elements of the density matrix). The precise formulation of the relationship between the two is a subject for future research.